Soft mean spherical approximation for dusty plasma liquids: One-component Yukawa systems with plasma shielding

P. Tolias,[1] S. Ratynskaia,[1] and U. de Angelis[2]
[1]*Space and Plasma Physics, Royal Institute of Technology, Stockholm, SE-100 44, Sweden*
[2]*INFN Sezione di Napoli, Naples, 80126, Italy*
(Received 16 September 2014; published 3 November 2014)

The structure and thermodynamics of strongly coupled dusty plasmas are investigated with the soft mean spherical approximation. This integral theory approach is analytically solvable for Yukawa pair interactions yielding a closed-form solution for the direct correlation function. The pair correlation function, the structure factor, and basic thermodynamic quantities are calculated for a wide range of parameters. Exact consistency between the "energy"-"virial" thermodynamic routes and approximate consistency between the "energy"-"compressibility" paths is demonstrated. Comparison with extensive molecular dynamics results is carried out and a remarkable agreement from the Coulomb limit to the strongly screened limit is revealed. The soft mean spherical approximation is concluded to be particularly well suited for the study of dusty plasma liquids, uniquely combining simplicity and accuracy.

DOI: 10.1103/PhysRevE.90.053101 PACS number(s): 52.27.Lw, 52.27.Gr, 05.20.Jj, 52.25.Kn

I. INTRODUCTION

Yukawa systems are pair-additive many-body systems, where the pair-potential energy has the form $U(r) = (Q^2/r)\exp[-(r/\lambda_{\rm scr})]$, with Q the charge of the particles and $\lambda_{\rm scr}$ a screening length accounting for the polarization of the medium. A species constituting a multicomponent system is considered strongly coupled when the mean pair-potential energy starts exceeding the kinetic energy, which also implies the onset of strong correlations and the existence of short- or long-range order. Common realizations of strongly coupled Yukawa systems include colloidal suspensions (complex fluids) [1] and dusty plasmas (complex plasmas) [2].

For dusty plasmas, it has been extensively assumed in the literature that the dust-dust interaction energy is of the Yukawa type with $\lambda_{\rm scr} = \lambda_{\rm D}$, where $\lambda_{\rm D}$ is the plasma Debye length, i.e., of the Debye-Hückel type. We point out that this might hold approximately true in some parameter regimes [3], but it is certainly not valid in all dusty plasma configurations, even when they are isotropic [4]. Nevertheless, in the Debye-Hückel case, the thermodynamics of strongly coupled dusty plasmas can be conveniently described in terms of two dimensionless quantities: the *coupling parameter* Γ defined roughly as the ratio of the unscreened Coulomb potential energy at the Wigner-Seitz radius to the kinetic energy, the *normalized screening parameter* κ defined as the ratio of the Wigner-Seitz radius to the plasma Debye length. Mathematically, we have

$$\Gamma = \frac{Q_{\rm d}^2}{dT_{\rm d}}, \quad \kappa = \frac{d}{\lambda_{\rm D}}, \tag{1}$$

where $d = (4\pi n_{\rm d}/3)^{-1/3}$ is the Wigner-Seitz radius with $n_{\rm d}$ the dust density, $Q_{\rm d}$ is the dust charge, and $T_{\rm d}$ is the dust temperature in energy units. In what follows, we use the dimensionless parameters (Γ,κ) instead of the quantities $(n_{\rm d},T_{\rm d})$ as independent thermodynamic variables. Throughout this paper, we shall employ the broader term Yukawa for the Debye-Hückel potential ($\lambda_{\rm scr} = \lambda_{\rm D}$).

Following the discovery of dusty plasma crystals [5,6], a large number of experimental, numerical, and theoretical investigations have focused on the static and dynamical properties of strongly coupled dusty plasmas, mainly in the crystal phase, for both finite and bulk systems, two-dimensional or three-dimensional [2,4,7]. In the last years, the interest in the properties of liquid dusty plasmas has also been considerably growing [7,8].

In this work, we study the thermodynamics and structure of Yukawa dusty plasma liquids by solving the Ornstein-Zernike equation within the soft mean spherical approximation. This analytical approach is known to uniquely combine accuracy and simplicity. Thus, it appears to be well suited for an extensive investigation of the parameter space of the Yukawa potential. Such an investigation is particularly timely: the Plasma Kristall Experiment-4 (PK-4) launch for the International Space Station (ISS) is scheduled within 2014 and the first experiments will be carried out in the beginning of 2015 [9]. PK-4 experiments on dusty plasma liquids are considered as prioritized basic experiments.

The paper is organized as follows: In Sec. II, we introduce the theoretical model of the dusty plasma system and the integral equation method known as soft mean spherical approximation. Within this approximation's closure conditions, the Ornstein-Zernike equation is analytically solved. It is shown that the problem reduces to the solution of one nonlinear equation and a detailed methodology is outlined for its numerical solution that is valid in the entire (Γ,κ) parameter space. In Sec. III, the pair correlation function is numerically calculated and the structure factor is analytically calculated. A rapidly converging and accurate numerical recipe is suggested for the Laplace inversion necessary for the pair correlation function computation. In Sec. IV, the basic thermodynamic quantities are calculated. Comparison with the most recent extensive molecular dynamics simulations reveals a remarkable agreement in all the ranges where numerical data are available. Moreover, we demonstrate an exact thermodynamic consistency between the "energy" and "virial" thermodynamic paths and an approximate thermodynamic consistency between the "energy" and "compressibility" paths. In Sec. V, the Coulomb limit $\kappa = 0$ is considered. The limiting solution is analytically acquired by means of successive Taylor expansions, the pair correlation functions are numerically

computed from the structure factor with the aid of Fourier inversion, and a comparison with molecular dynamics results once again reveals excellent agreement. In Sec. VI, we discuss issues related to the existence of physical solutions of the nonlinear equation, to the level of accuracy of the soft mean spherical approximation results, to the validity of the Yukawa potential for dusty plasmas and to experimental results in microgravity. We also briefly compare our approach with other integral theory methods that had been previously applied to Yukawa dusty plasma systems. Finally, in Sec. VII we summarize the advantages of the soft mean spherical approximation.

II. SOFT MEAN SPHERICAL APPROXIMATION FOR ONE-COMPONENT YUKAWA SYSTEMS

We shall consider an idealized model of the dusty plasma medium. The system is assumed to be in thermodynamic equilibrium. The dust grains are considered to be point particles and when immersed in the medium they acquire a constant nonfluctuating negative charge $Q_d = -Z_d e$ by absorbing plasma fluxes. The system is quasineutral, i.e., $n_i = n_e + Z_d n_d$. The plasma particles are solely responsible for the screening with the resulting pair potential being of the Yukawa type $\phi(r) = (Q_d/r)\exp[-(r/\lambda_D)]$, where λ_D is the plasma Debye length $\lambda_D^{-2} = \lambda_{De}^{-2} + \lambda_{Di}^{-2}$ with $\lambda_{De} = \sqrt{T_e/(4\pi e^2 n_e)}$ the electron Debye length and $\lambda_{Di} = \sqrt{T_i/(4\pi e^2 n_i)}$ the ion Debye length. Moreover, the only strongly coupled element of the system concerns dust-dust interactions. Therefore, in this aspect, the system can be considered as one component. We shall study its structure and thermodynamics by means of integral equation theory [10].

Thermodynamic equilibrium implies that the system is characterized by a single temperature $T_d = T_i = T_e = T$. (In this work, the temperature is in energy units and β denotes the inverse temperature.) However, in the one-component system approximation, it is sufficient that the dust species is in thermodynamic equilibrium and the plasma species can have their own distinct temperatures. This is the standard situation in dusty plasma experiments realized in gas discharges, where the dust and ion species are equilibrated with the neutrals $T_d = T_i = T_n$, while the electron species is characterized by a much higher temperature $T_e \gg T_n$.

A. One-component system approximation

The Ornstein-Zernike (OZ) system of equations for multicomponent dusty plasmas has the general form [11]

$$h_{ij}(\boldsymbol{r}) = C_{ij}(\boldsymbol{r}) + \sum_\alpha n_\alpha \int h_{i\alpha}(|\boldsymbol{r}-\boldsymbol{r}'|)C_{\alpha j}(\boldsymbol{r}')d^3r',$$

where $\{i, j, \alpha\}$ denote the different particle species $\{e, i, d\}$, $C_{ij}(\boldsymbol{r})$ is the direct correlation function between the "i-j" species, $h_{ij}(\boldsymbol{r}) = g_{ij}(\boldsymbol{r}) - 1$ is the total correlation function, and $g_{ij}(\boldsymbol{r})$ is the pair correlation function also known as radial distribution function. The OZ equations for the plasma species can be dropped owing to the large value of the plasma parameter, while $h_{ij}(\boldsymbol{r}) = h_{ji}(\boldsymbol{r})$ and $C_{ij}(\boldsymbol{r}) = C_{ji}(\boldsymbol{r})$ due to action-reaction reciprocity. These arguments reduce the OZ system to three equations for $h_{dd}(\boldsymbol{r})$, $h_{di}(\boldsymbol{r})$, and $h_{de}(\boldsymbol{r})$. When assuming $g_{di}(\boldsymbol{r}) = g_{de}(\boldsymbol{r}) = 1$, the only strongly coupled element of the system concerns dust-dust interactions and the OZ system is self-consistently further reduced to a single equation for the dust component. In such a three-dimensional spherically symmetric one-component system, the Ornstein-Zernike equation has the form [11,12]

$$h(r) = C(r) + n_d \int h(|\boldsymbol{r}-\boldsymbol{r}'|)C(r')d^3r', \qquad (2)$$

where we introduced the compact notations $C_{dd}(r) = C(r)$, $h_{dd}(r) = h(r)$, and $g_{dd}(r) = g(r)$.

In a series of papers [13–16], Hamaguchi *et al.* performed systematic and unprecedentedly accurate molecular dynamic simulations of strongly coupled dusty plasma systems of the Yukawa type. Their simulations focused on dust-dust interactions since for plasma-dust interactions the linearized solution of the Poisson-Boltzmann system was assumed in their electrostatic field calculations [13]. This assumption corresponds to the linear Debye-Hückel approximation for electron-dust and ion-dust interactions, for which we have $g_{de}(r) = 1 - \beta U_{de}(r)$, $g_{di}(r) = 1 - \beta U_{di}(r)$ with $U_{de}(r) = -e\phi(r)$, $U_{di}(r) = e\phi(r)$. These pair correlation functions lead to nonzero direct correlation functions $C_{de}(r)$ and $C_{di}(r)$, which implies a nonzero indirect plasma-dust contribution to the dust-dust pair correlation function, that is not accounted for in Eq. (2). In assuming a one-component Yukawa system, we implicitly assume that the contributions of the terms $n_e \int h_{de}(|\boldsymbol{r}-\boldsymbol{r}'|)C_{de}(\boldsymbol{r}')d^3r'$ and $n_i \int h_{di}(|\boldsymbol{r}-\boldsymbol{r}'|)C_{di}(\boldsymbol{r}')d^3r'$ to dust-dust correlations are negligible. This is a reasonable assumption, provided that dust-plasma coupling can be regarded as considerably weak. We note that this assumption had been followed by all integral equation theoretical studies that compare their results with the Hamaguchi *et al.* numerical experiments.

B. Soft mean spherical approximation

The Ornstein-Zernike equation can be viewed as the definition of the direct correlation function. Apparently, Eq. (2) cannot be simultaneously solved for both $C(r)$ and $g(r)$ and an approximate closure scheme is necessary. We shall employ the soft mean spherical approximation (SMSA) [17–20] which can be considered as an adaptation of the mean spherical approximation (MSA) of hard-core potentials [21–26] to soft-core potentials. It comprises of three closure conditions.

(1) *The hard-core condition*. Since we address a system consisting of charged point particles interacting via the Yukawa pair potential, the dust grains are assumed to possess no impenetrable core. However, dense systems always act as if their pair potentials possess an effective hard-core diameter, which we denote as R_h. Therefore, the system behaves as if the pair potential has the form $\phi(r) = \infty, r < R_h$ and $\phi(r) = (Q_d/r)\exp[-(r/\lambda_D)], r > R_h$. The former branch is equivalent to the closure condition $g(r) = 0, r < R_h$.

(2) *The asymptotic condition*. It can be shown from diagrammatic analysis that, for fluids away from their bulk critical region, the decay of the direct correlation function follows the relation $\lim_{r\to\infty} C(r) = -\beta U(r)$ [27]. It is assumed that the asymptotic form is valid in the whole region extending beyond

the hard-core diameter. This leads to the closure condition $C(r) = -\beta U(r), r > R_h$.

(3) *The continuity condition*. In contrast to genuine hard spheres, owing to the smooth continuous nature of the Yukawa pair potential, the pair correlation function should not possess a jump discontinuity at the hard-core parameter. Consequently, we have $g(r = R_h^+) = g(r = R_h^-)$ which leads to the closure condition $g(r = R_h^+) = 0$.

A fundamental result of diagrammatic analysis states that the general closure relation for the OZ equation reads as $g(r) = \exp[-\beta U(r) + h(r) - C(r) + B(r)]$, where $B(r)$ is the bridge function that corresponds to the sum of all elementary diagrams in the cluster expansion [28]. It is customary to differentiate between integral theory approaches by their corresponding bridge function values. For instance, in the hypernetted chain approximation, the contribution of the elementary diagrams is neglected and $B_{\rm HNC}(r) = 0$ [29]. Within this context, it is straightforward to prove that the set of SMSA closure conditions is equivalent to a bridge function which diverges negatively for $r \leqslant R_h$ and is given by [18]

$$B_{\rm SMSA}(r) = -h(r) + \ln[g(r)], \ \forall\, r\,.$$

The first two closure conditions are sufficient for us to acquire an analytical solution of the OZ equation. Actually, these conditions constitute the MSA closure for hard-core potentials. For such potentials, the hard-core diameter is predefined, which is not the case for soft-core potentials. Therefore, an additional condition is necessary to uniquely determine R_h. Such is the continuity condition, first suggested by Gillan [17].

In the limit of uncharged dust grains the mean spherical approximation reduces to the Percus-Yevick (PY) approximation for the hard-sphere fluid [30]. In fact, the mathematical methods we shall employ for the solution of the problem are extensions of techniques originally developed for the solution of the PY approach. We point out that, in the case of hard-sphere fluids, the agreement of the MSA internal energy with numerical simulation results is excellent at relatively large densities. However, MSA suffers from thermodynamic inconsistency [31]. As we shall see in the following sections, this is not the case for the SMSA [32].

C. Dimensionless quantities for Yukawa interactions

We shall employ dimensionless spatial coordinates of the form $x = r/R_h$. In this rescaled coordinate system, the closure condition switching point lies at $x = 1$. Moreover, it is convenient to define the dimensionless quantity $\eta = (\pi/6)\, n_d R_h^3$ that is known as the hard-sphere packing fraction. The physical range of the packing fraction can be considered as $\eta \in [0,1]$. However, stricter upper limits can be found by considering that the largest fraction of space that can be occupied by equal rigid spheres is given by $\sqrt{2}\pi/6 \simeq 0.740\,48$.

The normalized Yukawa pair interaction energy $\beta U(r) = (Z_d^2 e^2/Tr)\exp[-(r/\lambda_D)]$ can be rewritten as $\beta x U(x) = \gamma e^{-\lambda x}$. The new dimensionless parameters are defined by $\gamma = (d/R_h)\,\Gamma$ and $\lambda = (R_h/d)\,\kappa$. They can be expressed as functions solely of the packing fraction via

$$\gamma(\eta) = \tfrac{1}{2}\eta^{-1/3}\Gamma\,, \quad \lambda(\eta) = 2\eta^{1/3}\kappa\,.$$

Finally, we define the parameter $k = \sqrt{24\eta\gamma}$ whose square shall frequently appear in our calculations.

D. Analytical solution of the SMSA for one-component Yukawa systems

The OZ equation with the above closure conditions can be solved analytically either with the Wertheim [33–35] or with the Baxter factorization methods [36–38]. The Baxter method involves a transformation of the OZ equation with the aid of Fourier analysis and the Wiener-Hopf factorization technique, it is a powerful method especially when generalizations are imperative [37,38], but it is rather complicated for simple potentials. Therefore, we shall employ the Wertheim method, which is based on Laplace transforms. Mathematically, the method is intricate but the solution for Coulomb and exponential-type interactions is quite established [19,24,39], hence, we shall only sketch the main steps. We first define the functions $C_0(x) = C(x) + \beta U(x)$, $G(x) = xg(x)$, $F(x) = xC_0(x)$, the Laplace transforms $\widetilde{G}(s) = \int_1^\infty e^{-sx} G(x)dx$, $\widetilde{F}(s) = \int_1^\infty e^{-sx} F(x)dx$, and the parameters $v_\lambda = -k^2\widetilde{G}(\lambda)$ and $A_\lambda = -\left(\lambda^2/k^2\right) v_\lambda(v_\lambda + 2\gamma\lambda)$. Moreover, we employ the compact notations $G_n = G^{(n)}(1^+)$ and $\Upsilon_n = F^{(n)}(1^-)$ for the derivatives of the nth order, which implies that the continuity condition can be rewritten as $\Upsilon_0 = 0$. Finally, we define the parameter

$$a = 1 - 24\eta \int_0^\infty x^2 C(x)dx\,. \tag{3}$$

Employing azimuthally expanded two-center bipolar coordinates for the convolution term and spherical coordinates for the remaining terms, the Laplace transform of the OZ equation can be compactly written as

$$\begin{aligned} s^2\widetilde{K}(s)\widetilde{G}(s) &= \widetilde{H}(s)\,,\\ \widetilde{K}(s) &= 1 + \frac{12\eta}{s}[\widetilde{F}(s) - \widetilde{F}(-s)] - \frac{k^2}{s^2-\lambda^2}, \\ \widetilde{H}(s) &= s^2\widetilde{F}(s) + a - \frac{\gamma s^2}{s+\lambda} + \frac{s^2 v_\lambda}{s^2-\lambda^2}. \end{aligned} \tag{4}$$

We proceed with introducing the function

$$\widetilde{L}(s) = \widetilde{G}(s)\widetilde{H}(-s) = \frac{\widetilde{H}(s)\widetilde{H}(-s)}{s^2\widetilde{K}(s)}\,. \tag{5}$$

By the analyticity properties of the Laplace transforms and the evenness of $\widetilde{L}(s)$ it is inferred that the latter is a meromorphic function with a double pole at $s = 0$ and single poles at $s = \pm\lambda$. Subtracting from $\widetilde{L}(s)$ the principal part of its Laurent series, we can construct a function that is holomorphic over the whole complex plane

$$\widetilde{M}(s) = \widetilde{L}(s) - \frac{a}{s^2} - \frac{A_\lambda}{s^2-\lambda^2}\,.$$

The function $\widetilde{M}(s)$ is an entire function that behaves as a constant at infinity, with a limit equal to $-\Upsilon_0^2$ which under the continuity condition is zero. Therefore, by an extension of Liouville's theorem, we obtain $\widetilde{M}(s) = 0$ or, equivalently,

$$\widetilde{L}(s) = \frac{a}{s^2} + \frac{A_\lambda}{s^2-\lambda^2}. \tag{6}$$

For a Yukawa potential, employing $\Upsilon_0 = 0$ and the evenness of $\widetilde{L}(s)$ it is straightforward to prove that $G_n = -\Upsilon_n$ for $n \leqslant 6$. For $\mathrm{Re}\{s\} \to \infty$, Eqs. (5) and (6) can be expanded in even negative powers of s to yield

$$\widetilde{L}(s) \sim \frac{\Upsilon_1^2}{s^2} + \frac{2\Upsilon_1\Upsilon_3 - \Upsilon_2^2}{s^4} + \frac{\Upsilon_3^2 - 2\Upsilon_2\Upsilon_4 + 2\Upsilon_1\Upsilon_5}{s^6},$$

$$\widetilde{L}(s) \sim \frac{a + A_\lambda}{s^2} + \frac{\lambda^2 A_\lambda}{s^4} + \frac{\lambda^4 A_\lambda}{s^6},$$

respectively, with the higher order terms involving unknown functions $G_n, n \geqslant 7$. Equating the coefficients of equal powers we end up with three equations that are complemented by the continuity condition, i.e.,

$$\begin{aligned} &\Upsilon_1^2 = a + A_\lambda\,, \quad 2\Upsilon_1\Upsilon_3 - \Upsilon_2^2 = \lambda^2 A_\lambda\,, \\ &\Upsilon_3^2 - 2\Upsilon_2\Upsilon_4 + 2\Upsilon_1\Upsilon_5 = \lambda^4 A_\lambda. \end{aligned} \tag{7}$$

When considering the inverse Laplace transforms for $x \leqslant 1$, products of the form $\widetilde{G}(s)\widetilde{f}(s)$ are encountered. Let $f(x)$ be a well-behaved function and $\widetilde{f}(s)$ be its Laplace transform, by the hard-core assumption we obtain $\mathcal{L}^{-1}\{\widetilde{G}(s)\widetilde{f}(s)\} = 0$. Combining this property with Eqs. (4) and (5), we have $\mathcal{L}^{-1}\{H(s)/s^2\} = \mathcal{L}^{-1}\{-\left(12\eta/s^3\right)L(s)\}$, which can be inverted to yield the direct correlation function for $x \leqslant 1$. The final result in the whole range is

$$\begin{aligned} C(x) &= -\frac{\gamma}{x}e^{-\lambda x},\ x \geqslant 1 \\ C(x) &= -a - \left(\frac{v_\lambda^2}{4\gamma\lambda} + \frac{v_\lambda}{2}\right)\lambda x - \frac{1}{2}\eta a x^3 - v_\lambda\frac{1 - e^{-\lambda x}}{\lambda x} \\ &\quad + \frac{v_\lambda^2}{2\gamma\lambda}\frac{\cosh(\lambda x) - 1}{\lambda x},\ x \leqslant 1\,. \end{aligned} \tag{8}$$

E. Simplification of the system of nonlinear equations

In order to complete the SMSA solution of the OZ equation, we need to determine the unknowns $(\eta\,, a\,, v_\lambda)$. The equations available are the definition of the parameter "a," the continuity condition, and the three asymptotic expansion equations. The system of nonlinear equations appears to be overdetermined, however, in the SMSA, only one of Eqs. (7) is independent. Employing Eq. (3) which is linear in "a" we obtain a $a(v_\lambda,\eta)$ expression. Combining with $\Upsilon_0 = 0$, which is linear in "a" and quadratic in v_λ, we end up with an expression for $v_\lambda(\eta)$. Therefore, we can acquire analytic expressions of the form $a(\eta)\,, v_\lambda(\eta)$, thus reducing the problem to solving only one nonlinear equation for η. The results can be conveniently rewritten as

$$v_\lambda = \frac{-B \pm \sqrt{B^2 - 4AC}}{2A}, \quad a = a_2 v_\lambda^2 + a_1 v_\lambda + a_0,$$

where for the quadratic coefficients we have

$$A = \left(1 + \frac{1}{2}\eta\right)a_2 - \frac{\cosh\lambda - 1}{2\gamma\lambda^2} + \frac{1}{4\gamma},$$

$$B = \left(1 + \frac{1}{2}\eta\right)a_1 + \frac{1 - e^{-\lambda}}{\lambda} + \frac{\lambda}{2},$$

$$C = \left(1 + \frac{1}{2}\eta\right)a_0 - \gamma e^{-\lambda},$$

while for the "a" coefficients we have

$$a_0 = \frac{1}{1 - 8\eta - 2\eta^2}\left[1 + \frac{k^2 e^{-\lambda}}{\lambda}\left(1 + \frac{1}{\lambda}\right)\right],$$

$$a_1 = \frac{24\eta}{1 - 8\eta - 2\eta^2}\frac{1}{\lambda}\left[\left(1 + \frac{1}{\lambda}\right)\frac{e^{-\lambda}}{\lambda} - \frac{1}{\lambda^2} + \frac{1}{2} + \frac{\lambda^2}{8}\right],$$

$$a_2 = \frac{12\eta}{1 - 8\eta - 2\eta^2}\frac{1}{\gamma\lambda^2}\left(\frac{\cosh\lambda - 1}{\lambda^2} - \frac{\sinh\lambda}{\lambda} + \frac{1}{2} + \frac{\lambda^2}{8}\right).$$

Despite these major simplifications, we point out the remaining equation, one of Eqs. (7), is highly nonlinear in η. This nonlinearity stems mostly from the $\lambda(\eta)$ and $\gamma(\eta)$ dependencies. The solution of this equation will permit us to find the packing fraction η for any given (Γ,κ) pair.

F. Solution of the nonlinear equation for the packing fraction

By inspecting the above equations, it is apparent that the coefficients a_j and thus the parameter "a" tend to infinity at the roots $\eta_c = -2 \pm (3/2)\sqrt{2}$ of the quadratic polynomial $1 - 8\eta - 2\eta^2$. Moreover, the positive root $\eta_c = -2 + (3/2)\sqrt{2} \simeq 0.121\,32$ is a physically acceptable solution for η. As critical coupling parameter Γ_{crit}, we define the value of the coupling parameter for which the packing fraction corresponds to η_c. Owing to the simple pole at $\eta = \eta_c$, an exact relation for Γ_{crit} cannot be derived but its numerical value can be approached with arbitrary precision. As will be explained later, the importance of Γ_{crit} lies in the fact that it provides a rule that determines for which coupling parameters the quadratic relation for v_λ switches from the "+" to the "−" sign in front of the discriminant.

For each screening parameter κ, there is a unique value of Γ_{crit}. For $0 \leqslant \kappa \leqslant 5$, the corresponding values of Γ_{crit} can be found in Table I. In the same table, we quote the values of the coupling parameter at the liquid-solid phase transition Γ_{melt} as found by molecular dynamics simulations [13–16]. The Γ_{melt}

TABLE I. The coupling parameter at the melting point Γ_{melt} as found by molecular dynamics simulations for different κ [14–16]. The critical coupling parameter Γ_{crit} of the SMSA at the critical packing fraction η_c.

κ	Γ_{melt}	Γ_{crit}
0.0	171.8	10.26786
0.2	173.5	10.36600
0.4	178.6	10.66366
0.6	187.1	11.1695
0.8	199.6	11.8984
1.0	217.4	12.8721
1.2	243.3	14.121
1.4	268.8	15.682
2.0	440.1	22.804
2.6	758.9	35.39
3.0	1185	48.61
3.6	2378	80.31
4.0	3837	113.7
4.6	8609	194.5
5.0	15060	279.2

values will serve as the upper Γ limit in our calculations of thermodynamic quantities.

Following, we present the most important constituents of the systematic method we developed for the solution of the nonlinear equation. (i) Consistency of the integral equation solution. In the whole (Γ,κ) parameter space, use of any of the nonlinear equations [see Eqs. (7)] leads to the same η solution. In order to reduce the computation time, it is preferable to use $\Upsilon_1^2 = a + A_\lambda$ due to its simplicity. (ii) The packing fraction for $\Gamma > \Gamma_{\rm crit}$. Since $\eta(\Gamma,\kappa)$ is a monotonically increasing function of the coupling parameter, the physical solution corresponds to $\eta > \eta_c$. It is found by employing v_λ^-, i.e., the v_λ equation with the minus sign in front of the discriminant, whereas, in this range, the v_λ^+ equation typically leads to the unphysical solution η_c for η. Finally, note that the numerical solution is nearly independent of the first guess $\eta_{\rm in}$. (iii) The packing fraction for $\Gamma < \Gamma_{\rm crit}$. The physical solution corresponds to $\eta < \eta_c$. It is found by employing v_λ^+, i.e., the v_λ equation with the plus sign in front of the discriminant, whereas, in this range, the v_λ^- equation typically leads to unphysical complex solutions for η. For coupling parameters corresponding to the liquid state, the numerical solution is nearly independent of the first guess $\eta_{\rm in}$. On the contrary, for coupling parameters corresponding to the gaseous state, the numerical solution depends on the first guess $\eta_{\rm in}$. This implies that multiple solutions exist in the acceptable interval $[0,1]$, the physical solution corresponds to the extremum of the internal energy and always ensures that the monotonicity of (η, v_λ) with respect to Γ is preserved. (iv) The Coulomb plasma case. In the $\kappa \to 0$ limit, the quadratic expression for v_λ turns to linear, whereas all $1 - 8\eta - 2\eta^2$ denominators cancel out. As a consequence, there is no sign-switching condition to be determined by $\Gamma_{\rm crit}$ and η_c no longer represents a pole. Nevertheless, the $\Gamma_{\rm crit}$ value is still provided in Table I since it is essential for the determination of a fitted expression $\Gamma_{\rm crit}(\kappa)$. The Coulomb plasma limit will be examined separately in Sec. V.

Employing the tabulated values, we can find a least-square expression for $\Gamma_{\rm crit}(\kappa)$. We use the notation $\Gamma_{\rm crit}(0) = \Gamma_{\rm crit}^{\rm OCP}$ and seek for the best-fit parameters of the expression

$$\Gamma_{\rm crit}(\kappa) = \Gamma_{\rm crit}^{\rm OCP}\frac{e^\kappa}{1 + b\kappa + (c/2)\kappa^2}. \tag{9}$$

This expression was chosen considering the expansion $e^x \simeq 1 + x + x^2/2 + \ldots$ due to the clustering of the results for small κ around $\kappa = 0$. We end up with $b = 1.339\,42$, $c = -0.179\,331$, and a mean absolute relative error $e_r = 2.11\,\%$. The result is plotted in Fig 1. Surprisingly, $\Gamma_{\rm melt}(\kappa)$ can be shown to obey a similar functional dependence but with $b' = 1.206\,71$, $c' = -0.427\,72$, and $e_r' = 4.96\,\%$.

Finally, in Fig. 2 we plot $\eta(\Gamma,\kappa)$. Notice that within the range of parameters studied we always have $\eta < 0.4$, i.e., the packing fraction is always smaller than the upper mathematical bound. Moreover, notice that for large values of Γ close to the melting line the plots nearly overlap.

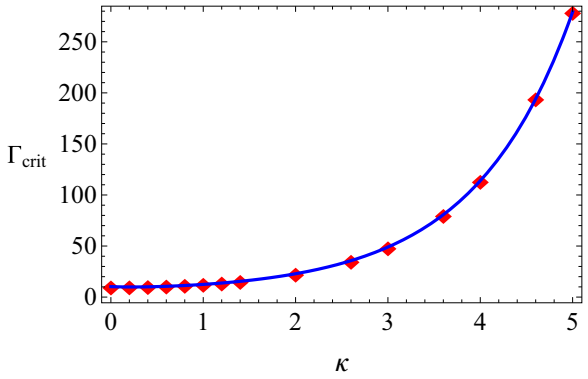

FIG. 1. (Color online) Plot of the least-square fit for $\Gamma_{\rm crit}(\kappa)$ together with the numerical data of Table I.

III. CALCULATION OF REDUCED DISTRIBUTION FUNCTIONS

A. Pair correlation function

The determination of the direct correlation function in the whole range of x formally completes the solution of the SMSA. This allows the computation of the pair correlation function in the whole range. We first calculate the Laplace transform of $F(x) = xC_0(x)$. We rewrite the piecewise function $C(x)$ in terms of Heaviside step functions, i.e., $C(x) = C_1(x)\mathrm{H}(x-1) + C_2(x)\mathrm{H}(1-x)$, where $C_1(x)$ denotes the upper branch and $C_2(x)$ the lower branch. This leads to $F(x) = x\,[C_2(x) + \beta U(x)]\,[1 - \mathrm{H}(x-1)]$ and the Laplace transform

$$\begin{aligned}\widetilde{F}(s) = &-\frac{\eta a}{2}\left(\frac{24}{s^5} - \frac{24e^{-s}}{s^5} - \frac{24e^{-s}}{s^4} - \frac{12e^{-s}}{s^3} - \frac{4e^{-s}}{s^2} - \frac{e^{-s}}{s}\right)\\ &+ \frac{v_\lambda}{\lambda}\left(-\frac{1}{s} + \frac{e^{-s}}{s} - \frac{e^{-s-\lambda} - 1}{s+\lambda}\right)\\ &+ \frac{v_\lambda^2}{2\gamma\lambda^2}\left(-\frac{1}{s} + \frac{e^{-s}}{s} - \frac{e^{-s}(s\cosh\lambda + \lambda\sinh\lambda) - s}{s^2 - \lambda^2}\right)\end{aligned}$$

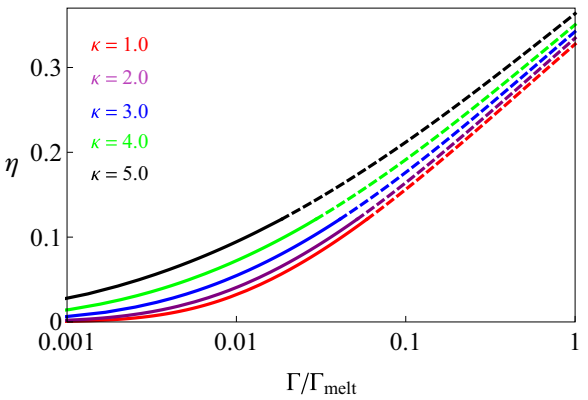

FIG. 2. (Color online) The packing fraction η as a function of $\Gamma/\Gamma_{\rm melt}$, calculated with the SMSA. Results for different values of κ. The lines switch from continuous to dashed at η_c, i.e., when the sign in front of the discriminant of v_λ switches. (The top curve corresponds to $\kappa = 5.0$ and the bottom curve corresponds to $\kappa = 1.0$.)

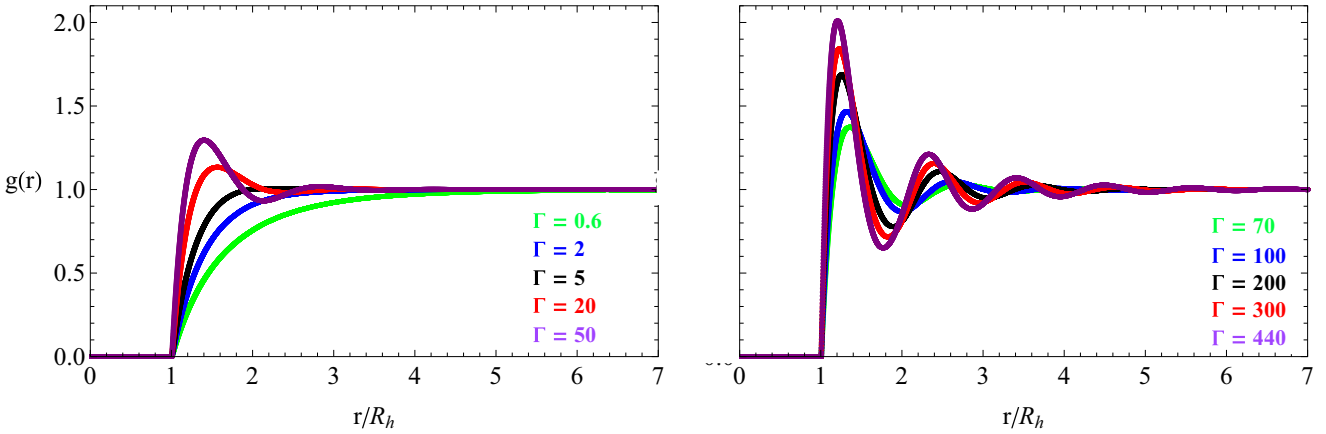

FIG. 3. (Color online) The pair correlation function $g(r)$ for $\kappa = 2.0$ and varying values of Γ as a function of the distance normalized by the hard-core diameter ($r/R_{\rm h}$). See also Ref. [42]. (In the left column, the top curve corresponds to $\Gamma = 50$ and the bottom curve corresponds to $\Gamma = 0.6$. In the right column, the top curve corresponds to $\Gamma = 440$ and the bottom curve corresponds to $\Gamma = 70$.)

$$-\left(\frac{v_\lambda^2}{4\gamma}+\frac{\lambda v_\lambda}{2}\right)\left(\frac{2}{s^3}-\frac{2e^{-s}}{s^3}-\frac{2e^{-s}}{s^2}-\frac{e^{-s}}{s}\right)$$
$$-a\left(\frac{1}{s^2}-\frac{e^{-s}}{s^2}-\frac{e^{-s}}{s}\right)-\gamma\frac{e^{-s-\lambda}-1}{s+\lambda}. \qquad (10)$$

The Laplace transform of $G(x) = xg(x)$ can now be found by solving Eq. (4) for $\widetilde{G}(s)$:

$$\widetilde{G}(s)=\frac{\widetilde{F}(s)+\frac{a}{s^2}-\frac{\gamma}{s+\lambda}+\frac{v_\lambda}{s^2-\lambda^2}}{1+\frac{12\eta}{s}[\widetilde{F}(s)-\widetilde{F}(-s)]-\frac{k^2}{s^2-\lambda^2}}. \qquad (11)$$

Finally, $g(x)$ can be calculated by carrying out the inverse Laplace transform

$$g(x)=\frac{1}{x}\mathcal{L}^{-1}\{\widetilde{G}(s)\}=\frac{1}{2\pi\imath x}\int_{\gamma-\imath\infty}^{\gamma+\imath\infty}e^{sx}\widetilde{G}(s)ds\,. \qquad (12)$$

Unfortunately, a closed-form expression for Eq. (12) does not exist. Therefore, a point-to-point Laplace inversion needs to be carried out numerically. Owing to the complex nature of the Bromwich contour, it is preferable to implement specialized Laplace inversion algorithms rather than resort to typical numerical integration routines. After trials with a number of algorithms (Stehfest, Piessens, Crump methods, etc.), the Durbin method [40,41] proved by far the most successful, combining fast convergence with high accuracy in the whole (κ,Γ) parameter space. Note that a reliable way to check the efficiency of inversion comes from the hard-sphere closure condition and the asymptotic behavior of the pair correlation function of liquids. The density of the inversion points was chosen to be equal to 1000 per one x unit, we also have $x_{\rm in} = 10^{-3}$ and $\Delta x = 10^{-3}$.

In Fig. 3 we plot the pair correlation function as a function of the distance normalized by the hard-core diameter, for $\kappa = 2.0$ and varying values of Γ up to the melting point. See also Ref. [42]. For all cases, the efficiency of the Laplace inversion is apparent: there is no numerical noise, the condition $g(r) = 0$ for $r < R_{\rm h}$ is satisfied with high accuracy, and $g(r)$ tends to unity after a few hard-core diameters.

For the same parameters, in Fig. 4, we plot the pair correlation function as a function of the distance normalized by the cubic mean interparticle distance $\Delta = n_{\rm d}^{-1/3}$. See also Ref. [42]. Such plots are preferred in strongly coupled dusty plasmas experiments [43]. We notice the following: (i) In the limit of vanishing coupling parameter, the hard-core

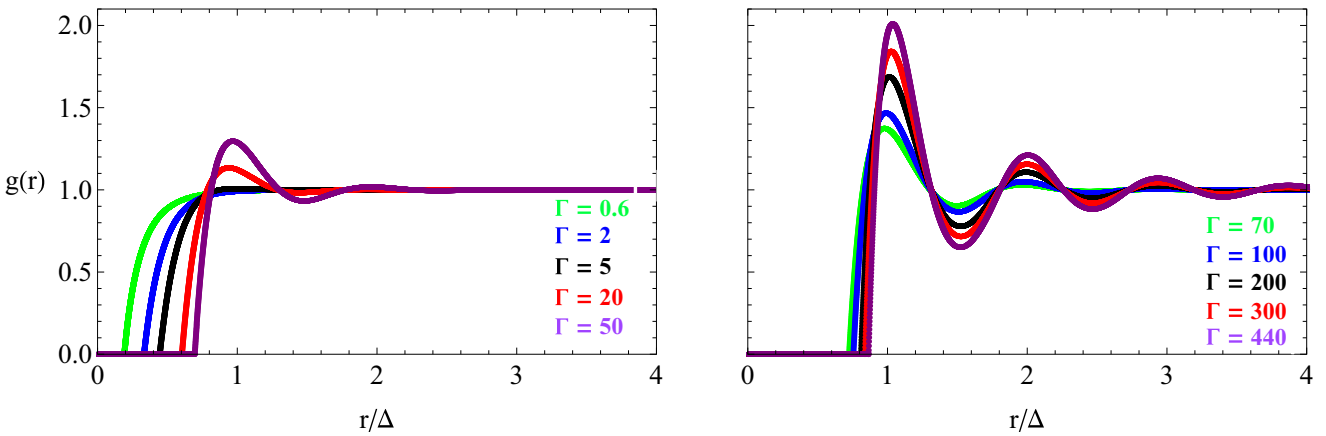

FIG. 4. (Color online) The pair correlation function $g(r)$ for $\kappa = 2.0$ and varying values of Γ as a function of the distance normalized by the cubic mean interparticle distance (r/Δ). See also Ref. [42]. (In the left column, the top curve corresponds to $\Gamma = 50$ and the bottom curve corresponds to $\Gamma = 0.6$. In the right column, the top curve corresponds to $\Gamma = 440$ and the bottom curve corresponds to $\Gamma = 70$.)

diameter tends to zero and $g(r)$ tends to unity in the whole range, which is the classical non-interacting gas limit. (ii) For low coupling parameters and as Γ increases, the hard-core diameter rapidly increases and $g(r)$ exhibits a clear nonlinear Debye-Hückel plus correlation hole character. (iii) Further increase of the coupling parameter leads to the formation of a shallow global maximum. Moreover, oscillations start to build up that are indicative of short-range order. (iv) For larger coupling parameters, the oscillations become more pronounced, namely, additional local maxima begin to shape, while the first maximum remains the global one with its amplitude slowly increasing. (v) For very large coupling parameters up to the melting point, the hard-core diameter is nearly constant and $g(r)$ exhibits a rapidly decaying oscillation pattern, a picture which persists also for $\Gamma > \Gamma_{\rm melt}$ in the supercooled liquid regime. (vi) Finally, for any Γ the position of global maximum is located very close to the interparticle distance $r = \Delta$, always slightly exceeding it.

The behavior of $g(r)$ with increasing Γ is similar regardless of the value of κ. This has been confirmed by systematically computing the pair correlation functions in the whole (κ,Γ) parameter space. The observed similarity hints that for the Yukawa-SMSA there probably exists a modified coupling parameter whose value alone determines the pair correlation function instead of the (Γ,κ) pair [44]. The task of identification of such a parameter will be undertaken in future work.

B. Structure factor

The structure factor is defined by the relation $S(\boldsymbol{k}) = 1 + n_{\rm d}\int [g(r)-1]\, e^{-\imath \boldsymbol{k}\cdot\boldsymbol{r}} d^3r = 1 + n_{\rm d}\widetilde{H}(\boldsymbol{k})$. Combining with the three-dimensional Fourier transform of the OZ equation $\widetilde{H}(\boldsymbol{k}) = \widetilde{C}(\boldsymbol{k}) + n_{\rm d}\widetilde{H}(\boldsymbol{k})\widetilde{C}(\boldsymbol{k})$ and introducing the normalized vector $\boldsymbol{q} = R_{\rm h}\boldsymbol{k}$, it is straightforward to acquire

$$S(\boldsymbol{q}) = \frac{1}{1 - n_{\rm d}\widetilde{C}(\boldsymbol{q})}\,.$$

Employing spherical coordinates, carrying out the azimuthal and polar integrations, and introducing dimensionless distances x, we end up with the expression

$$S(q) = \frac{1}{1 - (24\eta/q)\int_0^\infty x C(x)\sin(qx)dx}\,. \qquad (13)$$

The structure factor can now be expressed via elementary functions by substituting for the direct correlation function [Eq. (8)] and carrying out the remaining integrations, which are trivial. In Fig. 5, we plot the structure factor for $\kappa = 2.0$ and various values of Γ. Notice that the long-wavelength limit of the structure factor $S(0) = \lim_{q\to 0} S(q)$ is not zero and depends on Γ. We will examine $S(0)$ in more detail in the next section, when calculating the inverse compressibility.

IV. CALCULATION OF THERMODYNAMIC QUANTITIES

The thermodynamic quantities of interest are the internal energy (U), the Helmholtz free energy (F), the pressure (P), and the inverse isothermal compressibility ($\mu_{\rm T}$). Since it is preferable to work with dimensionless intensive variables, we

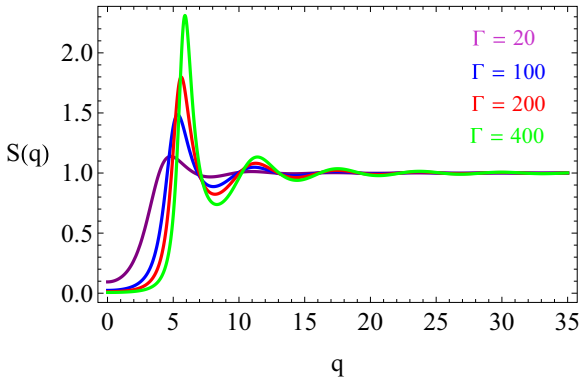

FIG. 5. (Color online) The structure factor $S(q)$ for $\kappa = 2.0$ and varying values of Γ as a function of the normalized wave number $q = R_{\rm h}k$. (The top curve corresponds to $\Gamma = 400$ and the bottom curve corresponds to $\Gamma = 20$.)

define the reduced counterparts of these quantities via

$$u = \frac{U}{NT}\,,\quad f = \frac{F}{NT}\,,\quad p = \frac{P}{nT}\,,\quad \mu_{\rm p} = \frac{\mu_{\rm T}}{nT}\,.$$

Furthermore, it is convenient to define reduced excess quantities by subtracting the ideal gas contribution, i.e., for a thermodynamic quantity X we define its reduced excess counterpart by $x_{\rm ex} = (X - X_{\rm id})/X_{\rm norm}$.

We shall only focus on the aforementioned thermodynamic quantities since we aim to perform a numerical study of the thermodynamic consistency aspects of the SMSA. However, we remind the reader that other intensive quantities such as the reduced entropy (s), the specific heat capacities at constant volume and constant pressure ($c_{\rm p}$, $c_{\rm v}$), or quantities such as the high frequency bulk and shear modulus (B_∞, G_∞) can be easily calculated through thermodynamic equations and pair correlation functions, respectively [31,45].

A. Reduced excess internal energy due to dust-dust interactions

The reduced excess internal energy due to dust-dust interactions is given by $u_{\rm ex}^{\rm dd} = (1/2)\,\beta n_{\rm d}\int U(r)g(r)d^3r$. The introduction of spherical coordinates, normalized distances, and the Yukawa potential leads to $u_{\rm ex}^{\rm dd} = (1/2)\,k^2\int_0^\infty e^{-\lambda x} x g(x)dx = (1/2)\,k^2\widetilde{G}(\lambda)$. Overall, we get

$$u_{\rm ex}^{\rm dd}(\Gamma,\kappa) = -\frac{v_\lambda}{2}\,. \qquad (14)$$

Since v_λ is one of the unknowns of the SMSA system of equations, $u_{\rm ex}^{\rm dd}$ can be directly calculated without knowledge of the pair distribution function.

Before proceeding to a comparison with the molecular dynamics (MD) simulations of Hamaguchi *et al.* [13–16], we need to consider the multicomponent nature of the dusty plasma system in the same manner. Assuming the validity of linear Debye-Hückel theory for electron-dust and ion-dust interactions, we have $g_{\rm de}(r) = 1 + e\beta\phi(r)$, $g_{\rm di}(r) = 1 - e\beta\phi(r)$. As a consequence, the excess energy due to the presence of dust can be decomposed in three terms $u_{\rm ex}^{\rm d} = u_{\rm ex}^{\rm dd} + u_{\rm ex}^{\rm dp} + u_{\rm ex}^{\rm ds}$, where $u_{\rm ex}^{\rm dd}$ denotes the excess energy due to dust-dust interactions, $u_{\rm ex}^{\rm dp} = -(3/2)(\Gamma/\kappa^2)$ the excess energy due to dust interaction with the unperturbed quasineutral plasma

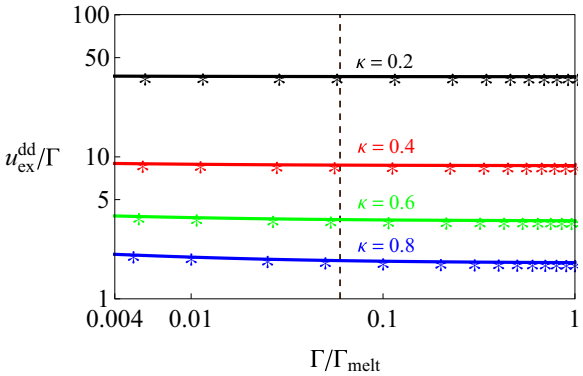

FIG. 6. (Color online) The reduced excess internal energy due to dust-dust interactions u_{ex}^{dd} normalized by the coupling parameter Γ as a function of Γ/Γ_{melt}, calculated with the SMSA. The data points correspond to the MD results [14]. The vertical lines correspond to $\Gamma = \Gamma_{crit}/\Gamma_{melt}$, in order to identify the sign switching of the closed-form solution. Results for low κ.

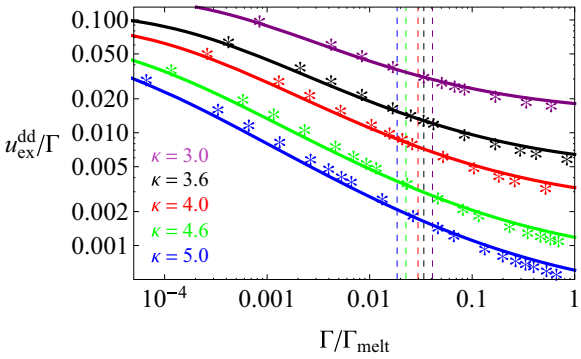

FIG. 8. (Color online) The reduced excess internal energy due to dust-dust interactions u_{ex}^{dd} normalized by the coupling parameter Γ as a function of Γ/Γ_{melt}, calculated with the SMSA. The data points correspond to the MD results [16]. The vertical lines correspond to $\Gamma = \Gamma_{crit}/\Gamma_{melt}$, in order to identify the sign switching of the closed-form solution. Results for high κ. (The top curve corresponds to $\kappa = 3.0$ and the bottom curve corresponds to $\kappa = 5.0$.)

background, and $u_{ex}^{ds} = -(1/2)\Gamma\kappa$ the excess energy due to dust interaction with the linear plasma sheath surrounding the grains.

The MD results tabulated in Refs. [14–16] correspond to u_{ex}^{d}. Notice that $u_{ex}^{dd} > 0$, whereas $u_{ex}^{dp}, u_{ex}^{ds}, u_{ex}^{d} < 0$, which implies that the dust-plasma terms are always dominating the dust-dust term. Therefore, only a comparison between the u_{ex}^{dd} terms is meaningful. Such a comparison is carried out in Figs. 6–8. The SMSA results exhibit a remarkable agreement with MD simulations from the strongly screened Yukawa regime up to the weakly screened Coulomb limit.

B. Reduced excess free energy due to dust-dust interactions

We begin with the Legendre transform definition of the Helmholtz free energy $F = U - TS$, that in terms of reduced quantities becomes $f = u - s$. Combining with the first order thermodynamic equation for the entropy $S = -(\partial F/\partial T)_{V,N}$ it is straightforward to prove that $u = -T(\partial f/\partial T)_n$. Introduction of the coupling parameter through the chain rule together with $\partial\Gamma/\partial T = -\Gamma/T$ leads to the expression $u_{ex} = \Gamma(\partial f_{ex}/\partial\Gamma)$ with a dust-dust interaction part $u_{ex}^{dd} = \Gamma\left(\partial f_{ex}^{dd}/\partial\Gamma\right)$. Since $f_{ex}^{dd}(0,\kappa) = 0$ by definition, the latter becomes

$$f_{ex}^{dd}(\Gamma,\kappa) = \int_0^{\Gamma} \left[u_{ex}^{dd}(\Gamma',\kappa)/\Gamma'\right] d\Gamma' . \qquad (15)$$

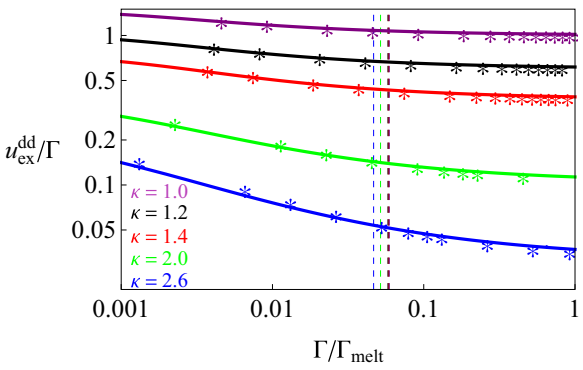

FIG. 7. (Color online) The reduced excess internal energy due to dust-dust interactions u_{ex}^{dd} normalized by the coupling parameter Γ as a function of Γ/Γ_{melt}, calculated with the SMSA. The data points correspond to the MD results [14–16]. The vertical lines correspond to $\Gamma = \Gamma_{crit}/\Gamma_{melt}$, in order to identify the sign switching of the closed-form solution. Results for intermediate κ. (The top curve corresponds to $\kappa = 1.0$ and the bottom curve corresponds to $\kappa = 2.6$.)

The above formula is numerically implemented in the following way: (i) Let Γ_1 be the lowest coupling parameter for which the excess free energy is evaluated, typically $\Gamma_1 = 10^{-4}\Gamma_{melt}$. We choose $\Gamma_0 = 10^{-2}\Gamma_1$ and calculate $f_{ex}^{dd}(\Gamma,\kappa) = f_{ex}^{dd}(\Gamma_0,\kappa) + \int_{\Gamma_0}^{\Gamma}[u_{ex}^{dd}(\Gamma',\kappa)/\Gamma']d\Gamma' \simeq \int_{\Gamma_0}^{\Gamma}[u_{ex}^{dd}(\Gamma',\kappa)/\Gamma']d\Gamma'$, which is a highly accurate approximation since $f_{ex}^{dd}(\Gamma,\kappa) > f_{ex}^{dd}(\Gamma_1,\kappa) \gg f_{ex}^{dd}(\Gamma_0,\kappa)$. (ii) Due to the lack of a closed-form expression for u_{ex}^{dd} as a function of Γ, an integrable interpolating function is constructed by piecewise Hermite interpolation. The density of $u_{ex}^{dd}(\Gamma_i,\kappa)$ points is chosen to be high, in order to ensure that the $f_{ex}^{dd}(\Gamma,\kappa)$ value is independent of the interpolating polynomial employed. (iii) The numerical integration is carried out with the Newton-Cotes quadrature rule. Due to the polynomial nature of the interpolation, all alternative integration algorithms that have been tested, such as the trapezoidal rule or the Clenshaw-Curtis quadrature, converged rapidly and yielded the same result.

It is important to compare the SMSA results with the fitting formula suggested by Hamaguchi *et al.* [13–16] to ensure that the very small deviations observed in the u_{ex}^{dd} values do not propagate additively in the f_{ex}^{dd} values owing to the integration. Motivated by variational hard-sphere approaches, Hamaguchi *et al.* [14] suggested the fitting formula $u_{ex}^{d}(\Gamma,\kappa) = a(\kappa)\Gamma + b(\kappa)\Gamma^s + c(\kappa) + d(\kappa)\Gamma^{-s}$ where $s = 1/3$ and $a(\kappa) = E(\kappa) + \delta a(\kappa)$ with $E(\kappa)$ the reduced Madelung energy. In order to avoid the divergence of the free energy at $\Gamma = 0$, they employed $f_{ex}^{d}(\Gamma,\kappa) = f_{ex}^{d}(1,\kappa) + \int_1^{\Gamma}[u_{ex}^{d}(\Gamma',\kappa)/\Gamma']d\Gamma'$. Therefore, for the dust-dust part

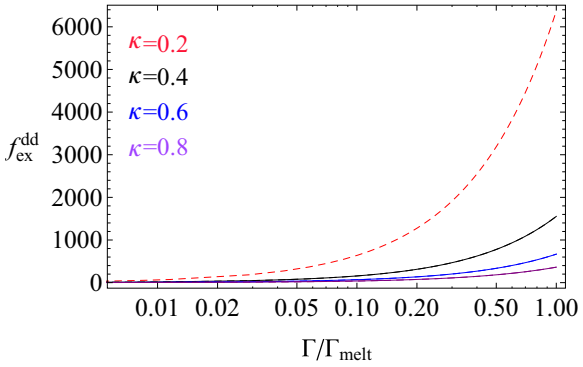

FIG. 9. (Color online) The reduced excess free energy due to dust-dust interactions f_{ex}^{dd} as a function of Γ/Γ_{melt} as calculated with the SMSA (solid line) and the Hamaguchi *et al.* fitting expression (dashed line). The SMSA results for low κ are totally indistinguishable from the MD results. (The top curve corresponds to $\kappa = 0.2$ and the bottom curve corresponds to $\kappa = 0.8$.)

we acquire

$$f_{ex}^{dd,MD}(\Gamma,\kappa) = f_{ex}^{d}(1,\kappa) + a(\kappa)(\Gamma - 1) + \frac{b(\kappa)}{s}(\Gamma^{s} - 1) + c(\kappa)\ln\Gamma + \frac{d(\kappa)}{s}(1 - \Gamma^{-s}) + \frac{3}{2}\frac{\Gamma}{\kappa^{2}} + \frac{1}{2}\Gamma\kappa\,.$$

For $k \leqslant 1$, the coefficients $a(\kappa), b(\kappa), c(\kappa), d(\kappa)$ are least-square fitted by even quartic polynomials and the coefficient $E(\kappa)$ is fitted by an even sixth order polynomial [15]. For $k > 1$, there exist no fitted expressions and the coefficient values are tabulated for each κ [16]. [Alternative polynomial fits for $k \leqslant 1$ have been proposed in Ref. [14]. We point out that there are misprints in some polynomial coefficients of $b(\kappa)$ and $d(\kappa)$: their sign is negative while it should be positive.]

The SMSA results for f_{ex}^{dd} are presented in Figs. 9–11. They are totally indistinguishable from the MD fitting expressions for low and intermediate screening parameters. As $\kappa > 3$ some very small deviations appear; these deviations seem to be slowly increasing with κ.

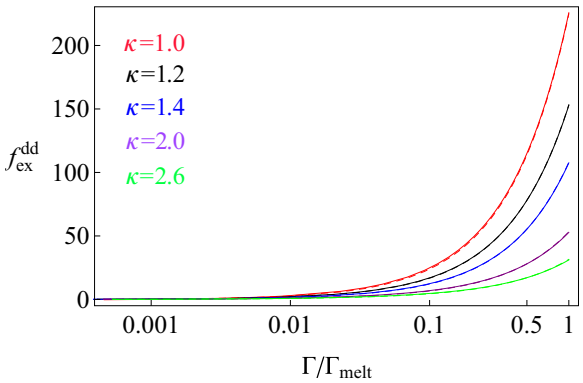

FIG. 10. (Color online) The reduced excess free energy due to dust-dust interactions f_{ex}^{dd} as a function of Γ/Γ_{melt} as calculated with the SMSA (solid line) and the Hamaguchi *et al.* fitting expression (dashed line). The SMSA results for intermediate κ are totally indistinguishable from the MD results. (The top curve corresponds to $\kappa = 1.0$ and the bottom curve corresponds to $\kappa = 2.6$.)

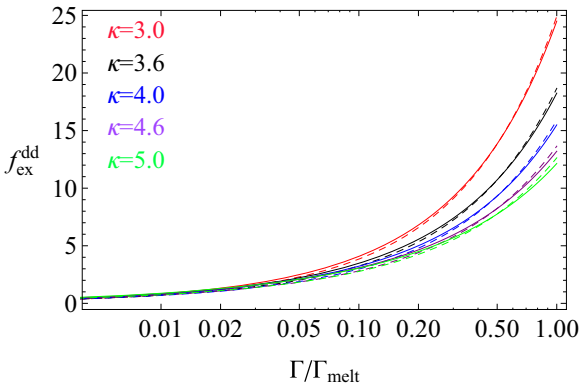

FIG. 11. (Color online) The reduced excess free energy due to dust-dust interactions f_{ex}^{dd} as a function of Γ/Γ_{melt} as calculated with the SMSA (solid line) and the Hamaguchi *et al.* fitting expression (dashed line). The SMSA results for high κ are practically indistinguishable from the MD results. (The top curve corresponds to $\kappa = 3.0$ and the bottom curve corresponds to $\kappa = 5.0$.)

C. Reduced excess pressure due to dust-dust interactions

In the *energy route* to the equation of state, the starting point is the first order thermodynamic equation for the pressure $P = -(\partial F/\partial V)_{T,N}$. In terms of reduced excess quantities, this expression can be rewritten as $p_{ex} = n\,(\partial f_{ex}/\partial n)$. We change to our dimensionless variables by using $n\,(\partial\kappa/\partial n) = -\kappa/3$ and $n\,(\partial\Gamma/\partial n) = \Gamma/3$. We also use Eq. (15) to end up with

$$p_{ex}^{dd}(\Gamma,\kappa) = -\frac{\kappa}{3}\frac{\partial f_{ex}^{dd}(\Gamma,\kappa)}{\partial\kappa} + \frac{u_{ex}^{dd}(\Gamma,\kappa)}{3}\,. \qquad (16)$$

Numerical calculation involves the computation of the first derivative of f_{ex}^{dd} with respect to κ. As demonstrated in the previous subsection, we can use the MD fitting function for $f_{ex}^{dd}(\Gamma,\kappa)$. However, the latter has a closed form with respect to κ only for $\kappa \leqslant 1$. We shall restrict ourselves to this range, when plotting results for the energy route equation of state.

In the *virial route* to the equation of state, the starting point is the virial expression. The reduced excess dust-dust interaction part reads as $p_{ex}^{dd}(\Gamma,\kappa) = -(1/6)\beta n_d \int r\,(dU/dr)\,g(r)d^3r$. Substituting for the interaction energy $U(r)$ and employing $x = r/R_h$ we have $p_{ex}^{dd}(\Gamma,\kappa) = (k^2/6)\int_0^\infty [xe^{-\lambda x} + \lambda x^2 e^{-\lambda x}]g(x)dx$. To further simplify this expression, it is useful to recall that for liquids the asymptotic value of the total correlation function $h(x) = g(x) - 1$ is zero, i.e., $\lim_{x\to\infty} h(x) = 0$. In the case of Yukawa interactions with $0 \leqslant \kappa \leqslant 5$, $h(x)$ drops to zero very rapidly, which implies that the integral can be evaluated in a relatively small integration range $x \in [0,x_0]$. Numerical results indicate that for liquids with $\Gamma/\Gamma_{melt} \in [10^{-4},1]$, we have $x_0 < 8$. On the other hand, for gases with $\Gamma/\Gamma_{melt} < 10^{-4}$, x_0 can attain much larger values due to the smallness of the hard-core diameter. Overall, we have

$$p_{ex}^{dd}(\Gamma,\kappa) = \frac{k^2}{6}\int_0^{x_0} [x + \lambda x^2]e^{-\lambda x}h(x)dx + \frac{k^2}{2\lambda^2}\,. \qquad (17)$$

The above formula is numerically implemented in the following way: (i) Since no closed-form expression exists for $g(x)$, an integrable interpolating function is constructed by piecewise Hermite interpolation. Within our working precision, spline

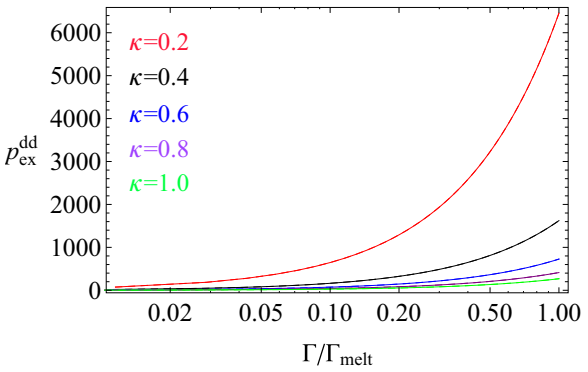

FIG. 12. (Color online) The reduced excess pressure due to dust-dust interactions p_{ex}^{dd} as a function of Γ/Γ_{melt} calculated from the virial route (solid line) and the energy route (dashed line), with the SMSA. Results for low κ. The curves are indistinguishable. (The top curve corresponds to $\kappa = 0.2$ and the bottom curve corresponds to $\kappa = 1.0$.)

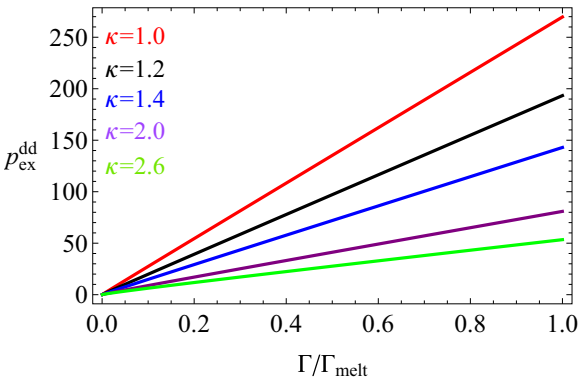

FIG. 13. (Color online) The reduced excess pressure due to dust-dust interactions p_{ex}^{dd} as a function of Γ/Γ_{melt} calculated from the virial route, with the SMSA. Results for intermediate κ. (The top curve corresponds to $\kappa = 1.0$ and the bottom curve corresponds to $\kappa = 2.6$.)

interpolation leads to exactly the same values for $p_{ex}^{dd}(\Gamma,\kappa)$ for all the cases considered, thus, ensuring a sufficient density of $g(x_i)$ points. (ii) The numerical integration is carried out with the Newton-Cotes quadrature rule.

In the *compressibility route* to the equation of state, the statistical mechanics formula for the inverse isothermal compressibility is integrated with respect to the density to yield the pressure. In order to avoid a tedious integration over the dimensionless variables (Γ,κ), it is preferable to compare the isothermal compressibilities as resulting from the different thermodynamic routes since their calculation involves only differentiations. Such a task is carried out in the following subsection.

In Fig. 12 we plot p_{ex}^{dd} from the "energy" and the "virial" route. For arbitrary stable soft potentials, it has been theoretically demonstrated that forcing the $g(r)$ continuity condition in the mean spherical approximation leads to thermodynamic consistency between the virial and energy equations of state [32]. This is confirmed in our numerical results for Yukawa interactions, where the two curves are indistinguishable for $\kappa \leqslant 1$. Such a comparison also serves as an internal consistency check and verifies that our numerical routines possess the desired accuracy. The virial equation of state for larger screening parameters can be found in Figs. 13 and 14.

Finally, the reduced excess pressure due to the presence of dust $p_{ex}^{d} = p_{ex}^{dd} + p_{ex}^{dp} + p_{ex}^{ds}$ can be rewritten as $p_{ex}^{d} = p_{ex}^{dd} - (3/2)(\Gamma/\kappa^2)$ since $p_{ex}^{dp} = -(3/2)(\Gamma/\kappa^2)$ and since, from the energy route, $p_{ex}^{ds} = 0$. The overall attractive interaction of dust with the plasma background is stronger in the whole parameter range and hence the quantity p_{ex}^{d} will always be negative.

D. Reduced excess inverse isothermal compressibility due to dust-dust interactions

In the *energy route* to the compressibility, we begin with the thermodynamic definition of the inverse isothermal compressibility $\mu_T = -V(\partial P/\partial V)_{T,N}$ or, equivalently, $\mu_T = n(\partial P/\partial n)_T$. We denote the reduced inverse isothermal compressibility as μ_p. Clearly, we have $\mu_p = (1/T)(\partial P/\partial n)_T$ and a dust-dust interaction part given by $\mu_p^{dd} = p_{ex}^{dd} + n(\partial p_{ex}^{dd}/\partial n)_T$. Using Eqs. (15) and (16), utilizing the Schwarz theorem of commutative partial derivatives, and employing the relations $n(\partial\kappa/\partial n) = -\kappa/3$ and $n(\partial\Gamma/\partial n) = \Gamma/3$, we end up with

$$\mu_p^{dd}(\Gamma,\kappa) = \frac{u_{ex}^{dd}(\Gamma,\kappa)}{3} - \frac{2\kappa}{9}\frac{\partial f_{ex}^{dd}(\Gamma,\kappa)}{\partial\kappa} + \frac{\kappa^2}{9}\frac{\partial^2 f_{ex}^{dd}(\Gamma,\kappa)}{\partial\kappa^2} - \frac{2\kappa}{9}\frac{\partial u_{ex}^{dd}(\Gamma,\kappa)}{\partial\kappa} + \frac{\Gamma}{9}\frac{\partial u_{ex}^{dd}(\Gamma,\kappa)}{\partial\Gamma}. \quad (18)$$

In the *statistical route* to the compressibility, we start with the well-known formula $T(\partial n/\partial P)_T = 1 + n\int h(r)d^3r$. From the definition of the structure factor and the Fourier transform of the OZ equation, the formula can be rewritten as $\mu_p = 1/[1 + n_d\int h(r)d^3r] = 1/S(0) = 1 - n_d\widetilde{C}(0)$. Employing Eq. (13), taking the long-wavelength limit and using $\lim_{q\to 0}[\sin(qx)/q] = x$, we have $\mu_p = 1 - 24\eta\int_0^\infty x^2 C(x)dx = a$. In the ideal gas limit, we have $h(x) = 0$, which leads to $\mu_p = 1$. Therefore, the above expression incorporates the ideal gas contribution, and subtracting it

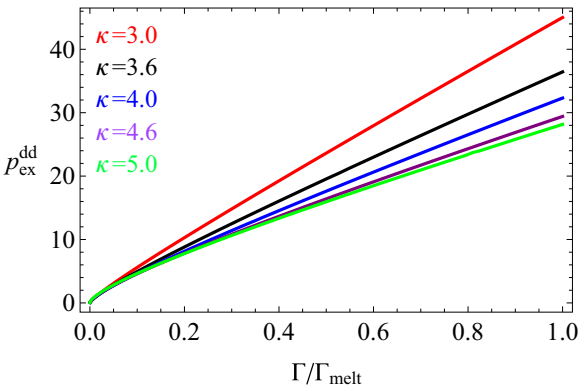

FIG. 14. (Color online) The reduced excess pressure due to dust-dust interactions p_{ex}^{dd} as a function of Γ/Γ_{melt} calculated from the virial route, with the SMSA. Results for high κ. (The top curve corresponds to $\kappa = 3.0$ and the bottom curve corresponds to $\kappa = 5.0$.)

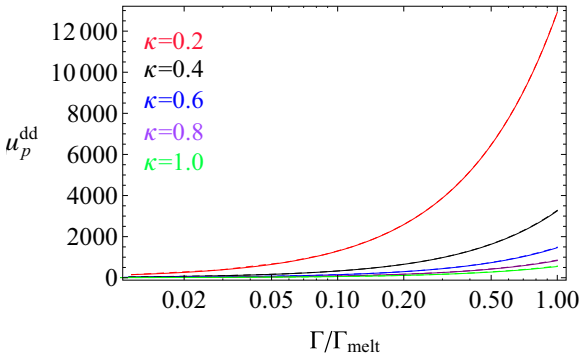

FIG. 15. (Color online) The reduced excess inverse isothermal compressibility $\mu_p^{dd}(\Gamma,\kappa)$ as a function of Γ/Γ_{melt} calculated from the statistical route (solid line) and the energy route (dashed line), with the SMSA. Results for low κ. The curves are practically indistinguishable. (The top curve corresponds to $\kappa = 0.2$ and the bottom curve corresponds to $\kappa = 1.0$.)

we get

$$\mu_p^{dd}(\Gamma,\kappa) = a - 1\,. \tag{19}$$

Notice that since "a" is one of the unknowns of the SMSA system of equations, μ_p^{dd} can be directly calculated without knowledge of the direct correlation function.

In Fig. 15, we plot μ_p^{dd} from the energy and the statistical route. It is clear that the two curves are practically indistinguishable for Yukawa interactions in the range $\kappa \leqslant 1$. We point out that such a thermodynamic consistency is not valid for any stable soft potential treated within the SMSA. Therefore, it can be considered as a peculiarity of the Yukawa potential in the range of κ studied. In Figs. 16 and 17, results for μ_p^{dd} that correspond to larger screening parameters are plotted (derived from the statistical route only).

Summing up, we have numerically demonstrated the approximate equivalence of the "energy," "virial," and "compressibility" routes to thermodynamics for the soft mean spherical approximation in the case of Yukawa interactions. Triple thermodynamic consistency is a highly desirable property that

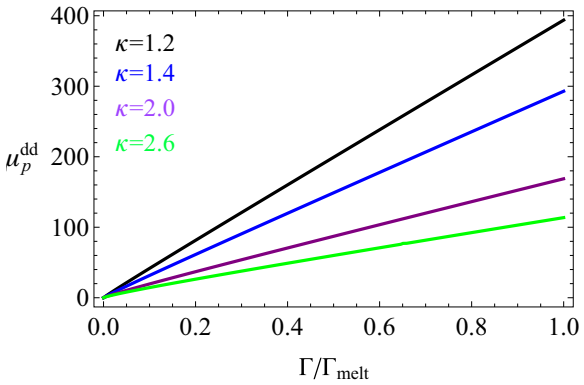

FIG. 16. (Color online) The reduced excess inverse isothermal compressibility $\mu_p^{dd}(\Gamma,\kappa)$ as a function of Γ/Γ_{melt} calculated from the statistical route with the SMSA. Results for intermediate κ. (The top curve corresponds to $\kappa = 1.2$ and the bottom curve corresponds to $\kappa = 2.6$.)

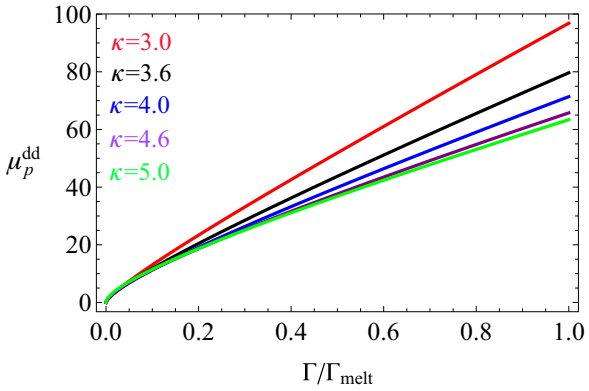

FIG. 17. (Color online) The reduced excess inverse isothermal compressibility $\mu_p^{dd}(\Gamma,\kappa)$ as a function of Γ/Γ_{melt} calculated from the statistical route with the SMSA. Results for high κ. (The top curve corresponds to $\kappa = 3.0$ and the bottom curve corresponds to $\kappa = 5.0$.)

rarely occurs in integral equation approximations of the liquid state theory. In fact, the results obtained via the three routes are typically different and they sometimes exhibit large variations [28].

V. CALCULATION OF THE COULOMB PLASMA LIMIT

Coulomb plasmas correspond to the $\kappa = 0$ limit of Yukawa plasmas. These systems are also known as one-component plasmas. Formally, they are defined as systems containing a single species of point charges embedded in a rigid, uniform background of neutralizing charges. Since the background remains uniform, there is no sheath formation around the point charges and the interaction potential is of the unscreened Coulomb type. Such systems have been thoroughly studied in the literature [31,46], hence, it is worth analyzing them also with the SMSA. Instead of solving the OZ system for the Coulomb potential, it is preferable to apply the limit of infinite screening length ($\lambda \to 0$) to the results of the previous sections. The limiting procedure is not straightforward; one has to deal with a number of removable divergencies that arise.

A. Direct correlation function

The direct correlation function in the Coulomb limit can be calculated from Eq. (8) by successive Taylor expansions with respect to the infinitesimally small parameter λ. First, we need to expand the coefficients a_0, a_1, a_2, A, B, C. In order to retain the necessary number of terms in the series expansions, it is useful to keep in mind that v_λ is divergent with $v_\lambda \propto \lambda^{-2}$:

$$a_2 = -\frac{\eta}{1-8\eta-2\eta^2}\frac{\lambda^2}{12\gamma}\left(1+\frac{\lambda^2}{40}\right),$$

$$a_1 = \frac{8\eta}{1-8\eta-2\eta^2}\left(1+\frac{\lambda^2}{10}\right),$$

$$a_0 = \frac{1}{1-8\eta-2\eta^2}\frac{k^2}{\lambda^2}\left(1+\frac{\lambda^2}{k^2}-\frac{\lambda^2}{2}\right),$$

$$A = -\frac{1-4\eta}{1-8\eta-2\eta^2}\frac{\lambda^2}{48\gamma} - \frac{2-10\eta-\eta^2}{1-8\eta-2\eta^2}\frac{\lambda^4}{2880\gamma},$$
$$B = \frac{1+2\eta^2}{1-8\eta-2\eta^2} + \frac{5-16\eta+2\eta^2}{1-8\eta-2\eta^2}\frac{\lambda^2}{30},$$
$$C = \frac{1+\frac{1}{2}\eta}{1-8\eta-2\eta^2}\frac{k^2}{\lambda^2} + \frac{1-\gamma+\frac{1}{2}\eta-4\eta\gamma-4\eta^2\gamma}{1-8\eta-2\eta^2}.$$

The parameter v_λ corresponds to the solution of a quadratic equation $Av_\lambda^2 + Bv_\lambda + C = 0$, the $\pm$ sign in front of the discriminant adds a degree of ambiguity to our limiting procedure. Moreover, for $\lambda \to 0$ we have $A \to 0$ and the quadratic equation turns into a linear equation. We recall that when $B > 0$ the linear equation solution $-C/B$ is recovered from the plus sign quadratic solution, and when $B < 0$ the linear equation solution $-C/B$ is recovered from the minus sign quadratic solution. In both cases, we have the same factorized form $v_\lambda = -(B/2A)[1-(1-4AC/B^2)^{1/2}]$. Therefore, we shall only consider the $\lambda \to 0$ limit of this expression and disregard the $v_\lambda = -(B/2A)[1+(1-4AC/B^2)^{1/2}]$ solution. After some tedious algebra, we end up with

$$v_\lambda = -\frac{k^2}{\lambda^2} - D,$$
$$D = \frac{\left(1+\frac{1}{2}\eta\right)}{(1-\eta)(2\eta+1)} - \frac{(5+45\eta+3\eta^2+\eta^3)}{(2\eta+1)}\frac{\gamma}{5}.$$

Notice that all denominators of the form $1-8\eta-2\eta^2$ cancel out; this implies that η_c will not play any role in our solutions in contrast to the Yukawa case. For our convenience we also introduce the parameters $F = -a - v_\lambda$ and $G = F + D$:

$$F = -\frac{1}{2}\frac{\eta}{(1-\eta)(2\eta+1)} - \frac{(5+25\eta+7\eta^2-\eta^3)}{(2\eta+1)}\frac{\gamma}{5},$$
$$G = \frac{1}{(1-\eta)(2\eta+1)} - 2\gamma\frac{1+7\eta+\eta^2}{2\eta+1}.$$

We are now in the position to calculate the $\lambda \to 0$ limit of the direct correlation function $C(x)$ for $x \leqslant 1$. A large number of divergencies cancel out and we end up with

$$C(x) = -\frac{\gamma}{x}, \quad x \geqslant 1$$
$$C(x) = F + \tfrac{1}{6}k^2x^2 + \tfrac{1}{2}\eta G x^3 + \tfrac{1}{60}\eta k^2 x^5, \quad x \leqslant 1. \tag{20}$$

In order to complete the solution we also need to calculate the $\lambda \to 0$ limit of the system of equations [see Eq. (7)]. It is straightforward to acquire

$$\Upsilon_1^2 + G = 0, \quad 2\Upsilon_1\Upsilon_3 - \Upsilon_2^2 + k^2 = 0,$$
$$2\Upsilon_1\Upsilon_5 - 2\Upsilon_2\Upsilon_4 + \Upsilon_3^2 = 0. \tag{21}$$

B. Pair correlation function and the structure factor

The quantity $\widetilde{F}(s)$ can be determined either by Laplace transforming Eq. (20) or by taking the $\lambda \to 0$ limit of Eq. (10) since the Laplace operator can be interchanged with the limit operator. We have

$$\widetilde{F}(s) = \left(\frac{\gamma}{s} + \frac{F}{s^2} + \frac{k^2}{s^4} + \frac{12\eta G}{s^5} + \frac{12\eta k^2}{s^7}\right)$$
$$-\left(\gamma + F + \frac{1}{6}k^2 + \frac{1}{2}\eta G + \frac{1}{60}\eta k^2\right)\frac{e^{-s}}{s}$$
$$-\left(F + \frac{1}{2}k^2 + 2\eta G + \frac{1}{10}\eta k^2\right)\frac{e^{-s}}{s^2}$$
$$-\left(k^2 + 6\eta G + \frac{1}{2}\eta k^2\right)\frac{e^{-s}}{s^3}$$
$$-(k^2 + 12\eta G + 2\eta k^2)\frac{e^{-s}}{s^4}$$
$$-(12\eta G + 6\eta k^2)\frac{e^{-s}}{s^5} - 12\eta k^2\frac{e^{-s}}{s^6} - 12\eta k^2\frac{e^{-s}}{s^7}. \tag{22}$$

We continue with the $\lambda \to 0$ limit of Eq. (11) which yields

$$\widetilde{G}(s) = \frac{\widetilde{F}(s) - \frac{\gamma}{s} - \frac{F}{s^2}}{1 + \frac{12\eta}{s}[\widetilde{F}(s) - \widetilde{F}(-s)] - \frac{k^2}{s^2}}. \tag{23}$$

We can now calculate the pair correlation function after inverting the Laplace transform.

Surprisingly, for $\kappa = 0$, Laplace inversion of $\widetilde{G}(s)$ with the Durbin method does not yield satisfactory results. We shall follow an alternative approach based on Fourier inversion of the structure factor. The $S(q)$ expression is acquired by combining Eq. (13) with (20) . Extra caution should be taken in the calculation of the quantity $\int_1^{+\infty} C_1(x)\sin(qx)$ because in this case the $\lambda \to 0$ operator cannot be interchanged with the improper integral operator. Consequently, the integral $\int_1^\infty \gamma \sin(qx)dx$ does not converge, whereas $\lim_{\lambda\to 0}\int_1^\infty \gamma e^{-\lambda x}\sin(qx)dx = \gamma e^{-\lambda}(q\cos q + \lambda \sin q)/(q^2+\lambda^2) = \gamma(\cos q/q)$. Overall, we have

$$S^{-1}(q) = 1 - \frac{24\eta F}{q}I_1 - \frac{4\eta k^2}{q}I_3 - \frac{12\eta^2 G}{q}I_4$$
$$-\frac{2\eta^2 k^2}{5q}I_6 + k^2\frac{\cos q}{q^2}, \tag{24}$$

where we introduced the notation $I_n = \int_0^1 x^n \sin(qx)dx$. These integrals can be computed via the recursive relation $I_n = [(n\sin q - q\cos q)/q^2] - [n(n-1)/q^2]I_{n-2}$ with initial value $I_0 = (1-\cos q)/q$.

We can now invert the three-dimensional Fourier transform that defines the structure factor. After employing spherical coordinates and carrying out the angular integrations, we end up with

$$g(x) = 1 + \frac{1}{12\eta\pi}\frac{1}{x}\int_0^\infty q[S(q)-1]\sin(qx)dq. \tag{25}$$

This integral cannot be analytically evaluated and we have to proceed with numerical integration. However, we are encountering a rapidly oscillatory integrand in an infinite integration region. As a consequence, typical integration strategies do not yield realistic results. We employ a variant of the Levin collocation method [47] which proved to converge rapidly for all values of the coupling parameter. Plots of the

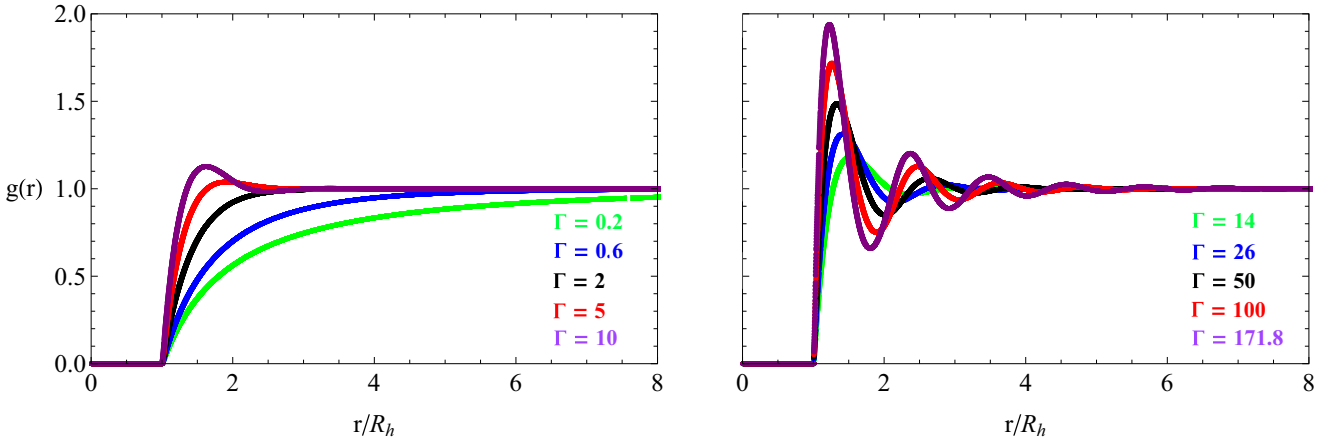

FIG. 18. (Color online) The pair correlation function $g(r)$ for Coulomb interactions and varying values of Γ as a function of the distance normalized by the hard-core diameter (r/R_h). See also Ref. [42]. (In the left column, the top curve corresponds to $\Gamma = 10$ and the bottom curve corresponds to $\Gamma = 0.2$. In the right column, the top curve corresponds to $\Gamma = 171.8$ and the bottom curve corresponds to $\Gamma = 14$.)

$g(r)$ as a function of r/R_h and r/Δ for various values of Γ can be found in Figs. 18 and 19, respectively. See also Ref. [42].

C. Reduced excess internal energy due to the presence of dust

Combining $v_\lambda = -(k^2/\lambda^2) - D$ with Eq. (14), we end up with the expression $u_{ex}^{dd} = D/2 + (k^2)/(2\lambda^2)$ for the reduced excess internal energy due to dust-dust interactions, which tends to infinity. We notice that $k^2/2\lambda^2 = (3/2)(\Gamma/\kappa^2)$. Hence, the divergence is canceled out exactly by the dust interaction with the plasma background $u_{ex}^{dp} = -(3/2)(\Gamma/\kappa^2)$. There is no sheath interaction term for a Coulomb plasma and the reduced excess internal energy due to the presence of dust is given by $u_{ex}^{d} = D/2$ or, equivalently,

$$u_{ex}^{d}(\Gamma) = \frac{1+\frac{1}{2}\eta}{(1-\eta)(4\eta+2)} - \frac{5+45\eta+3\eta^2+\eta^3}{(2\eta+1)}\frac{\gamma}{10}. \quad (26)$$

Hamaguchi *et al.* have also carried out MD simulations for Coulomb plasmas [14]. In Fig. 20, we plot both results. Once again, the SMSA remarkably agrees with the MD simulations.

VI. DISCUSSION

A. On the existence of physically acceptable hard-core diameters

Does the continuity condition of the SMSA guarantee the existence of a single physical solution for the packing fraction? Unfortunately, there is no guarantee that complementing the MSA closure conditions with the continuity condition will yield a physically acceptable solution for the packing fraction [32]. Moreover, there is the possibility that multiple physical solutions exist; in such a case, an additional criterion needs to be formulated for singling out one solution. Recall that we have encountered such a case for the Yukawa potential when $\Gamma \ll 1$. We also point out that there is no way of postulating a general criterion to be satisfied by arbitrary stable soft-core potentials for a physical packing fraction to emerge.

It has been rigorously proved by Rosenfeld [48] that the continuity condition is equivalent to an extremum condition for the excess internal energy when regarded as a function of the packing fraction. This had earlier been numerically

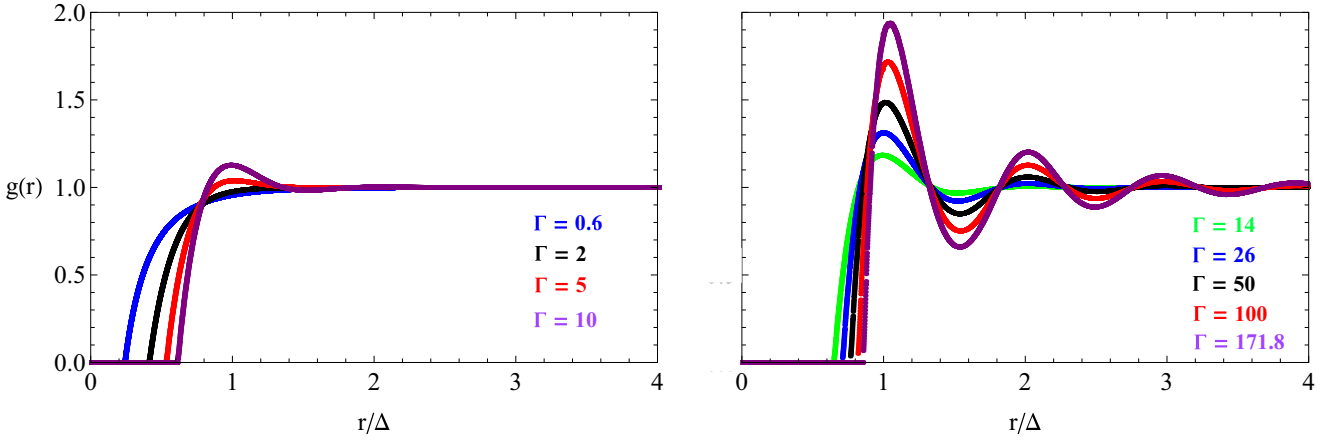

FIG. 19. (Color online) The pair correlation function $g(r)$ for Coulomb interactions and varying values of Γ as a function of the distance normalized by the cubic mean interparticle distance (r/Δ). See also Ref. [42]. (In the left column, the top curve corresponds to $\Gamma = 10$ and the bottom curve corresponds to $\Gamma = 0.6$. In the right column, the top curve corresponds to $\Gamma = 171.8$ and the bottom curve corresponds to $\Gamma = 14$.)

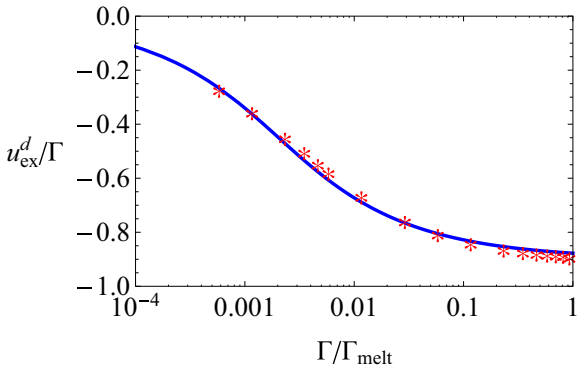

FIG. 20. (Color online) The reduced excess internal energy due to the presence of dust u^{d}_{ex} normalized by the coupling parameter Γ as a function of Γ/Γ_{melt}, as calculated with the SMSA for a Coulomb plasma. The data points correspond to the MD results [14].

observed for Coulomb plasmas [19,49]. This is not a global extremum condition, therefore, the possibility of no extremum or multiple local extrema cannot be excluded.

As an example, let us consider a bi-Yukawa potential with an attractive tail, which in dimensionless coordinates has the general form $\beta U(x) = (\gamma/x)(e^{-\lambda x} - \sigma e^{-\mu x})$ with $\lambda \gg \mu$ and $0 < \sigma \ll 1$. The solution of the MSA for such a potential has been derived in Ref. [39]. Complementing the MSA with the continuity equation, we end up with four unknowns $(\eta, a, v_\lambda, v_\mu)$ that satisfy four equations. Ultimately, this system can be transformed in a system of three nonlinear equations for (η, v_λ, v_μ). We have attempted to solve the system, but physically acceptable solutions cannot be found for η in the whole range of σ values.

B. On the level of accuracy of the SMSA

In Secs. IV and V, we showed that the SMSA solution leads to an accurate calculation of thermodynamic quantities. A pertinent question that arises concerns whether the level of SMSA accuracy is sufficient enough to provide reasonable results for Γ_{melt}. A rigorous answer to this question is formidable since it requires free energy calculations not only from the liquid side of the phase transition, but also from the solid side.

The answer can be sought in a less strict manner by computing the values of common freezing indicators for the SMSA at the exact values of Γ_{melt}, as calculated by Hamaguchi *et al.* [13–16]. Freezing indicators are quantitative phenomenological criteria for estimating the liquid-solid phase transition point and can be based on numerical simulations, experimental results, or theoretical extrapolations [50–53]. They refer to specific patterns in quantities such as the structure factor [54], the pair correlation function [55], the bridge function [56], or the multiparticle excess entropy [57] that remain nearly invariant along the liquid-solid coexistence curve. We point out that these criteria are approximate and there should be some skepticism concerning the existence of melting-line invariants that consider only one of the phases [58]. An extensive discussion on such criteria in the context of Yukawa dusty plasmas can be found in Ref. [59].

TABLE II. The values of the Hansen-Verlet freezing indicator S_{max} and the Raveché-Mountain-Streett freezing indicator $R = \min g(r)/\max g(r)$ calculated with the SMSA structure factors and correlation functions at the exact values of Γ_{melt}.

κ	S_{max}	R
0.0	2.3776	0.3400
0.2	2.3774	0.3402
0.4	2.3765	0.3399
0.6	2.3735	0.3397
0.8	2.3697	0.3393
1.0	2.3685	0.3382
1.2	2.3773	0.3353
1.4	2.3569	0.3371
2.0	2.3858	0.3234
2.6	2.3949	0.3180
3.0	2.4246	0.3086
3.6	2.4432	0.2987
4.0	2.4414	0.2946
4.6	2.4921	0.2806
5.0	2.5275	0.2715

The *Hansen-Verlet freezing rule* [54] is widely employed in the literature and is generally considered to be a robust freezing indicator, despite the fact that it originated from Monte Carlo simulations of Lennard-Jones fluids. It is based on the oscillating behavior of the structure factor near the liquid-solid phase transition and states that a three-dimensional liquid freezes when the first maximum of $S(k)$ exceeds 2.85. Note that, for any constant screening parameter, $S_{max}(\Gamma)$ is a monotonically increasing function. In Table II, we give the values of the SMSA S_{max} at the exact values of Γ_{melt}. We have $S_{max} < 2.85$ for all κ.

The *Raveché-Mountain-Streett freezing rule* [55] is another freezing indicator that was proposed on the basis of Monte Carlo results for classical Lennard-Jones fluids. It is based on the oscillating behavior of the pair correlation function near the liquid-solid phase transition and states that a three-dimensional liquid freezes where the amplitude ratio of the first nonzero minimum to the first maximum of $g(r)$ becomes less than 0.2. Note that, for any constant screening parameter, $R(\Gamma) = \min g(r)/\max g(r)$ is a monotonically decreasing function. In Table II, we give the values of the SMSA ratio R at the exact values of Γ_{melt}. We have $R > 0.2$ for all κ.

Taking into account the results of Table II, we conclude that the SMSA complies with these freezing criteria for values of the coupling parameter much higher than the actual Γ_{melt} (see also Table III). This unsatisfactory performance indicates that, despite its remarkable agreement with MD results and thermodynamic consistency, the SMSA does not possess the high accuracy required for the description of extremely sensitive phenomena such as liquid-solid phase transitions.

C. On the application of advanced integral equation approaches to Yukawa systems

It is worth comparing the SMSA approach with other integral equation approaches. In particular, the hypernetted chain approach [60] but also some of its advanced variants have

TABLE III. The coupling parameter at the melting point as found by molecular dynamics simulations and as found by applying the Hansen-Verlet freezing indicator to the SMSA, i.e., $\Gamma_{\rm melt}^{\rm SMSA} = \arg_{\Gamma}\{S_{\rm max}(\Gamma) = 2.85\}$.

κ	$\Gamma_{\rm melt}$	$\Gamma_{\rm melt}^{\rm SMSA}$
0.0	171.8	256.1
0.2	173.5	258.7
0.4	178.6	266.6
0.6	187.1	280.2
0.8	199.6	300.1
1.0	217.4	327.4
1.2	243.3	363.5
1.4	268.8	410.3
2.0	440.1	644.1
2.6	758.9	1129
3.0	1185	1721
3.6	2378	3426
4.0	3837	5584
4.6	8609	12030
5.0	15060	20438

been successfully applied to one-component Yukawa systems. Let us discuss these advanced approaches in further detail.

The empirically modified hypernetted chain approach, EMHNC, assumes an empirical bridge function of the form $B(r) = B_{\rm OCP}(\Gamma,r)f(\kappa)$, where $B_{\rm OCP}(\Gamma,r)$ is the OCP bridge function as extracted from Monte Carlo simulations of one-component plasmas [61] and $f(\kappa) = \exp(-\kappa^2/4)$ quantifies the effect of screening as determined through trial and error comparisons with molecular dynamics simulations of Yukawa plasmas [62]. Since the analytical form of the bridge function is prescribed, the EMHNC approach has the same numerical complexity with the HNC approach. It has been demonstrated [62] that the EMHNC solution for Yukawa systems possesses nearly exact thermodynamic consistency, exhibits excellent agreement with the MD results of Hamaguchi *et al.* and leads to calculated pair correlation functions nearly indistinguishable from the MD simulation results.

The variational modified hypernetted chain approach, VMHNC, is based on the hypothesis of approximate universality of the bridge functions, irrespective of the pair-potential [63–65]. It employs the analytical hard-sphere Percus-Yevick bridge function $B_{\rm PY}^{\rm HS}(r,\eta)$ with the value of the packing fraction determined by minimizing an appropriate free energy functional. Owing to this optimization procedure, the VMHNC approach exhibits exact consistency between the "energy"-"virial" thermodynamic routes and ensures that the "energy"-"compressibility" consistency is obeyed to a high degree of accuracy [66]. In contrast to the EMHNC approach, it is an entirely first-principles approach avoiding any fine tuning with the aid of simulation data. However, since the determination of $\eta_{\rm opt}$ can only be carried out iteratively, the computational load severely increases. It has been demonstrated [67] that the VMHNC solution for Yukawa systems is characterized by nearly exact thermodynamic consistency, excellent agreement with MD simulations and a strong performance with respect to the Hansen-Verlet freezing rule ($S_{\rm max} \simeq 3.05$) and other freezing indicators. It should be pointed out, though, that, due to the high nonlinearity of the coupled set of equations involved, the iterative scheme does not converge rapidly and stably in the whole (Γ,κ) parameter range [67].

The EMHNC and VMHNC approaches are expected to be more accurate than the SMSA, especially concerning calculations of the pair correlation function. However, originating from the hypernetted chain approach, they cannot be solved analytically. The analytically solvable SMSA can, thus, be considered optimal for fast and reliable calculations of thermodynamic quantities.

D. On realistic pair potentials for dusty plasmas

Our idealized model of the dusty plasma system assumes pointlike grains, interaction via a single Yukawa pair potential, screening provided only by the plasma particles and weakly coupled plasma species. These assumptions are not strictly valid for dusty plasmas. (i) Dust grains are not pointlike and possess an actual hard-core diameter. Our SMSA solution holds only when the effective hard-core diameter is larger than the grain diameter, i.e., when $R_{\rm h} > 2a$. (ii) Owing to strong ion-dust coupling, in the closest vicinity of the grain (for distances shorter than the nonlinear radius $R_{\rm nl}$) screening is nonlinear in character and the electrostatic potential can deviate from the simple Yukawa form [68,69]. Therefore, the present form of the SMSA is only valid when the nonlinear region is incorporated within the hard-core diameter. This leads to the condition $R_{\rm h} > 2R_{\rm nl}$. (iii) Within dense dust clouds, physical processes such as plasma absorption, dust charge fluctuations, and collisions with neutrals become collective in character and significantly alter the polarization cloud around each dust grain. These phenomena typically introduce a second characteristic length scale in the interactions that is larger than the Debye length: it leads to electrostatic potentials of the bi-Yukawa type [70–74]. (iv) Dust grains are not only screened by the plasma, but also participate in the shielding process; this implies that the screening length(s) will also depend on the coupling parameter. Equivalently, from a hydrodynamic test particle theory point of view, dust density perturbations have been shown to play an important role in determining the screening length(s) of the electrostatic potential, but not its functional form [75]. (v) For very large coupling parameters, it is inevitable that both ions and electrons are strongly coupled in their interactions with the dust grains. As a consequence, $g_{\rm ed}(r)$ and $g_{\rm id}(r)$ will not be of the Debye-Hückel type and could have an important effect on the dust-dust pair correlation function. This can only be tackled by considering the system of three OZ equations (still neglecting the three "pure plasma" OZ components).

Such an ideal picture of dusty plasmas was adopted in the numerical experiments of Hamaguchi *et al.* We follow these assumptions in order to perform a detailed comparison with MD results. Having demonstrated the remarkable agreement of the SMSA with MD, we can now reasonably assume that the SMSA solution is accurate for more realistic dusty plasma models, for which no numerical simulations exist. This shall be the subject of future work.

E. On experimental results for the pair correlation function

It is a well-known fact that ground experiments dedicated on strongly coupled dusty plasmas are characterized by a high degree of inhomogeneity and anisotropy, owing to the action of gravity and the strong electric fields necessary to compensate for it. On the other hand, under microgravity conditions, three-dimensional quasi-isotropic dusty plasmas can form. In principle, such experiments are ideal for direct measurements of the pair correlation function by analyzing the grain motion as recorded by CCD cameras. Microgravity investigations of the structural properties of dusty plasma liquids have been carried out in the ISS with the rf discharge Plasma Kristall Experiment-3 (PK-3) [43,76,77]. In these works, pair correlation functions were constructed from measurements.

The analysis of such experimental results is very challenging. In the rf discharge, an ellipsoidal void is formed in the center and dust grains are confined in its exterior regions. In these regions, the dust component can only be considered homogeneous within a few interparticle distances. Consequently, $g(r)$ only makes sense up to $r = 3\Delta$ [76]. Moreover, there are uncertainties in the determination of the Debye length and the dust charge, which lead to uncertainties in the calculation of (Γ, κ). Thus, a straightforward comparison with theory is a complicated issue.

Hopefully, the advanced particle manipulation capabilities of the combined dc/rf discharge Plasma Kristall Experiment-4 (PK-4) will lead to more extended homogeneous dusty plasma liquid regions [9,78,79]. The PK-4 launch for the ISS is scheduled for the end of October 2014 and the first experiments will be carried out in the beginning of 2015. Study of the thermodynamics and structure of dusty plasma liquids is listed as one of the prioritized basic experiments.

VII. SUMMARY AND CONCLUSIONS

In this work, we employed the soft mean spherical approximation in order to investigate the structure and thermodynamics of dusty plasma liquids under conditions when they can be considered as one-component Yukawa systems. Here, we shall briefly summarize the basic advantages of the SMSA application for Yukawa systems together with some of our main results.

(1) *Analytic solvability*. For exponential-type screening functions, the Ornstein-Zernike equation can be analytically solved within the SMSA closure conditions either with the Baxter or the Wertheim factorization techniques. For Yukawa systems, we have shown that the problem reduces to solving a 3×3 system of equations for the unknowns (a, v_λ, η). This system can be recast into a single nonlinear equation for the packing fraction, for the solution of which a systematic method has been developed.

(2) *Straightforward calculation of thermodynamic quantities*. Both the reduced excess internal energy and the reduced excess inverse isothermal compressibility are simple algebraic functions of the (a, v_λ) unknowns. Therefore, they can be readily calculated without the need to determine the pair correlation function or the structure factor.

(3) *Fast and accurate numerical calculation of the pair correlation function*. Rapidly converging and precise numerical techniques have been employed for a reliable calculation of the pair correlation function either by direct Laplace inversion or by Fourier inversion of the structure factor.

(4) *Triple thermodynamic consistency*. The SMSA "virial" and "energy" equations of state are identical, as theoretically proven in Ref. [32] for arbitrary stable pair potentials and numerically demonstrated here for Yukawa pair potentials. The SMSA "compressibility" equation of state has also been numerically demonstrated to be nearly identical to the other thermodynamic paths. This approximate triple thermodynamic consistency arises naturally without the need to artificially introduce additional parameters enforcing consistency.

(5) *Remarkable agreement with molecular dynamics simulations*. Comparison of the SMSA excess internal energy results with recent extensive molecular dynamics results, revealed a remarkable agreement in the whole (Γ,κ) parameter space, from the Coulomb plasma limit ($\kappa = 0$) to the strongly screened Yukawa limit ($\kappa = 5$).

In conclusion, we have demonstrated that the soft mean spherical approximation uniquely combines simplicity and accuracy. Consequently, it is the proper integral equation theory not only for an extensive investigation of the parameter space of the Yukawa potential, but also for application to more realistic strongly coupled dusty plasma models, for which no numerical simulations for comparison exist.

ACKNOWLEDGMENT

The authors acknowledge the support of the Swedish National Space Board.

[1] H. Löwen, Phys. Rep. **237**, 249 (1994); J. Phys.: Condens. Matter **13**, R415 (2001).
[2] G. E. Morfill and A. V. Ivlev, Rev. Mod. Phys. **81**, 1353 (2009).
[3] U. Konopka, G. E. Morfill, and L. Ratke, Phys. Rev. Lett. **84**, 891 (2000).
[4] V. E. Fortov, A. V. Ivlev, S. A. Khrapak, A. G. Khrapak, and G. E. Morfill, Phys. Rep. **421**, 1 (2005).
[5] J. H. Chu and Lin I, Phys. Rev. Lett. **72**, 4009 (1994).
[6] H. Thomas, G. E. Morfill, V. Demmel, J. Goree, B. Feuerbacher, and D. Möhlmann, Phys. Rev. Lett. **73**, 652 (1994).
[7] M. Bonitz, C. Henning, and D. Block, Rep. Prog. Phys. **73**, 066501 (2010).
[8] Z. Donko, G. J. Kalman, and P. Hartmann, J. Phys.: Condens. Matter **20**, 413101 (2008).
[9] V. Fortov, G. Morfill, O. Petrov, M. Thoma, A. Usachev, H. Hoefner, A. Zobnin, M. Kretschmer, S. Ratynskaia, M. Fink, K. Tarantik, Yu. Gerasimov, and V. Esenkov, Plasma Phys. Control. Fusion **47**, B537 (2005).
[10] J. A. Barker and D. Henderson, Rev. Mod. Phys. **48**, 587 (1976).
[11] R. Balescu, *Equilibrium and Nonequilibrium Statistical Mechanics* (Wiley, New York, 1975).

[12] H. L. Frisch and J. L. Lebowitz, *The Equilibrium Theory of Classical Fluids* (Benjamin, New York, 1964).
[13] S. Hamaguchi and R. T. Farouki, J. Chem. Phys. **101**, 9876 (1994).
[14] R. T. Farouki and S. Hamaguchi, J. Chem. Phys. **101**, 9885 (1994).
[15] S. Hamaguchi, R. T. Farouki, and D. H. E. Dubin, J. Chem. Phys. **105**, 7641 (1996).
[16] S. Hamaguchi, R. T. Farouki, and D. H. E. Dubin, Phys. Rev. E **56**, 4671 (1997).
[17] M. J. Gillan, J. Phys. C: Solid State Phys. **7**, L1 (1974).
[18] Y. Rosenfeld and N. W. Ashcroft, Phys. Rev. A **20**, 2162 (1979).
[19] G. Pastore, C. Nappi, U. de Angelis, and A. Forlani, Phys. Lett. A **78**, 75 (1980).
[20] U. de Angelis, A. Forlani, and M. Giordano, J. Phys. C: Solid State Phys. **13**, 3649 (1980).
[21] J. L. Lebowitz and J. K. Percus, Phys. Rev. **144**, 251 (1966).
[22] E. Waisman and J. L. Lebowitz, J. Chem. Phys. **52**, 4307 (1970).
[23] E. Waisman and J. L. Lebowitz, J. Chem. Phys. **56**, 3086 (1972).
[24] R. G. Palmer and J. D. Weeks, J. Chem. Phys. **58**, 4171 (1973).
[25] D. Henderson, G. Stell, and E. Waisman, J. Chem. Phys. **62**, 4247 (1975).
[26] D. Henderson and D. Boda, Mol. Phys. **109**, 1009 (2011).
[27] G. H. A. Cole, *An Introduction to the Statistical Theory of Classical Simple Dense Fluids* (Pergamon, Oxford, 1967).
[28] J.-P. Hansen and I. R. McDonald, *Theory of Simple Liquids* (Academic, New York, 2006).
[29] J. S. Rowlinson, Rep. Prog. Phys. **28**, 169 (1965).
[30] J. K. Percus and G. J. Yevick, Phys. Rev. **110**, 1 (1958).
[31] M. Baus and J.-P. Hansen, Phys. Rep. **59**, 1 (1980).
[32] Y. Rosenfeld, J. Stat. Phys. **37**, 215 (1984).
[33] M. S. Wertheim, Phys. Rev. Lett. **10**, 321 (1963).
[34] E. Thiele, J. Chem. Phys. **39**, 474 (1963).
[35] M. S. Wertheim, J. Math. Phys. **5**, 643 (1964).
[36] R. J. Baxter, Aust. J. Phys. **21**, 563 (1968).
[37] J. S. Høye and L. Blum, J. Stat. Phys. **16**, 399 (1977).
[38] L. Blum and J. S. Høye, J. Stat. Phys. **19**, 317 (1978).
[39] U. de Angelis, A. Forlani, and G. Masiello, Phys. Plasmas **7**, 3198 (2000).
[40] F. Durbin, Comput. J. **17**, 371 (1974).
[41] B. Davies and B. Martin, J. Comput. Phys. **33**, 1 (1979).
[42] See Supplemental Material at http://link.aps.org/supplemental/10.1103/PhysRevE.90.053101 for animations of the pair correlation function.
[43] V. E. Fortov, O. S. Vaulina, O. F. Petrov, V. I. Molotkov, A. M. Lipaev, V. M. Torchinsky, H. M. Thomas, G. E. Morfill, S. A. Khrapak, Yu. P. Semenov, A. I. Ivanov, S. K. Krikalev, A. Yu. Kalery, S. V. Zaletin, and Yu. P. Gidzenko, Phys. Rev. Lett. **90**, 245005 (2003).
[44] O. Vaulina, S. Khrapak, and G. Morfill, Phys. Rev. E **66**, 016404 (2002).
[45] N. K. Ailawadi, Phys. Rep. **57**, 241 (1980).
[46] S. Ichimaru, Rev. Mod. Phys. **54**, 1017 (1982).
[47] D. Levin, Math. Comput. **38**, 531 (1982).
[48] Y. Rosenfeld, J. Phys. C: Solid State Phys. **15**, L125 (1982).
[49] R. G. Palmer, J. Chem. Phys. **73**, 2009 (1980).
[50] G. P. Hoffmann and H. Löwen, J. Phys.: Condens. Matter **13**, 9197 (2001).
[51] B. A. Klumov, S. A. Khrapak, and G. E. Morfill, Phys. Rev. B **83**, 184105 (2011).
[52] S. A. Khrapak, B. A. Klumov, P. Huber, V. I. Molotkov, A. M. Lipaev, V. N. Naumkin, A. V. Ivlev, H. M. Thomas, M. Schwabe, G. E. Morfill, O. F. Petrov, V. E. Fortov, Yu. Malentschenko, and S. Volkov, Phys. Rev. E **85**, 066407 (2012).
[53] B. A. Klumov, J. Plasma Phys. **79**, 1125 (2013).
[54] J.-P. Hansen and L. Verlet, Phys. Rev. **184**, 151 (1969).
[55] H. J. Raveché, R. D. Mountain, and W. B. Streett, J. Chem. Phys. **61**, 1970 (1974).
[56] Y. Rosenfeld, Phys. Rev. A **24**, 2805 (1981).
[57] P. V. Giaquinta and G. Giunta, Phys. A (Amsterdam) **187**, 145 (1992).
[58] P. A. Monson and D. A. Kofke, in *Advances in Chemical Physics*, edited by I. Prigogine and S. A. Rice (Wiley, New York, 2000), Vol. 115, p. 113.
[59] B. A. Klumov, Phys.-Usp. **53**, 1053 (2010).
[60] G. J. Kalman, M. Rosenberg, and H. deWitt, J. Phys. IV (France) **10**, Pr5-403 (2000).
[61] H. Iyetomi, S. Ogata, and S. Ichimaru, Phys. Rev. A **46**, 1051 (1992).
[62] W. Daughton, M. S. Murillo, and L. Thode, Phys. Rev. E **61**, 2129 (2000).
[63] Y. Rosenfeld, J. Stat. Phys. **42**, 437 (1986).
[64] Y. Rosenfeld and N. W. Ashcroft, Phys. Rev. A **20**, 1208 (1979).
[65] Y. Rosenfeld, Phys. Rev. A **29**, 2877 (1984).
[66] L. E. Gonzalez, D. J. Gonzalez, and M. Silbert, Phys. Rev. A **45**, 3803 (1992).
[67] G. Faussurier, Phys. Rev. E **69**, 066402 (2004).
[68] V. N. Tsytovich, U. de Angelis, A. V. Ivlev, G. E. Morfill, and S. Khrapak, Phys. Plasmas **12**, 112311 (2005).
[69] S. Ratynskaia, U. de Angelis, S. Khrapak, B. Klumov, and G. E. Morfill, Phys. Plasmas **13**, 104508 (2006).
[70] V. N. Tsytovich, JETP Lett. **78**, 763 (2003).
[71] C. Castaldo, U. de Angelis, and V. N. Tsytovich, Phys. Rev. Lett. **96**, 075004 (2006).
[72] A. V. Filippov, A. G. Zagorodny, A. F. Pal, A. N. Starostin, and A. I. Momot, JETP Lett. **86**, 761 (2007).
[73] U. de Angelis, G. Regnoli, and S. Ratynskaia, Phys. Plasmas **17**, 043702 (2010).
[74] A. Yazdi, A. Ivlev, S. Khrapak, H. Thomas, G. E. Morfill, H. Löwen, A. Wysocki, and M. Sperl, Phys. Rev. E **89**, 063105 (2014).
[75] P. Tolias and S. Ratynskaia, Phys. Plasmas **20**, 023702 (2013).
[76] V. E. Fortov, O. S. Vaulina, O. F. Petrov, V. I. Molotkov, A. V. Chernyshev, A. M. Lipaev, G. Morfill, H. Thomas, H. Rotermell, S. A. Khrapak, Yu. P. Semenov, A. I. Ivanov, S. K. Krikalev, and Yu. P. Gidzenko, JETP **96**, 704 (2003).
[77] V. E. Fortov, O. S. Vaulina, O. F. Petrov, V. I. Molotkov, A. M. Lipaev, G. E. Morfill, H. Thomas, S. A. Khrapak, Yu. P. Semenov, and A. I. Ivanov, Plasma Phys. Control. Fusion **46**, B359 (2004).
[78] M. H. Thoma, M. A. Fink, H. Höfner, M. Kretschmer, S. A. Khrapak, S. V. Ratynskaia, V. V. Yaroshenko, G. E. Morfill, O. F. Petrov, A. D. Usachev, A. V. Zobnin, and V. E. Fortov, IEEE Trans. Plasma Sci. **35**, 255 (2007).
[79] S. Ratynskaia, M. Kretschmer, S. Khrapak, R. A. Quinn, M. H. Thoma, G. E. Morfill, A. Zobnin, A. Usachev, O. Petrov, and V. Fortov, IEEE Trans. Plasma Sci. **32**, 613 (2004).